2004-07-13

Unitary Space-Time Transmit Diversity for Multiple Antenna Self-Interference Suppression

Adam Lane Anderson
Brigham Young University - Provo

UNITARY SPACE-TIME TRANSMIT DIVERSITY FOR MULTIPLE ANTENNA SELF-INTERFERENCE SUPPRESSION

by

Adam L. Anderson

A thesis submitted to the faculty of

Brigham Young University

in partial fulfillment of the requirements for the degree of

Master of Science

Department of Electrical and Computer Engineering

Brigham Young University

August 2004

BRIGHAM YOUNG UNIVERSITY

GRADUATE COMMITTEE APPROVAL

of a thesis submitted by

Adam L. Anderson

This thesis has been read by each member of the following graduate committee and by majority vote has been found to be satisfactory.

Date	Michael A. Jensen, Chair
Date	Michael D. Rice
Date	Brian D. Jeffs

BRIGHAM YOUNG UNIVERSITY

As chair of the candidate's graduate committee, I have read the thesis of Adam L. Anderson in its final form and have found that (1) its format, citations, and bibliographical style are consistent and acceptable and fulfill university and department style requirements; (2) its illustrative materials including figures, tables, and charts are in place; and (3) the final manuscript is satisfactory to the graduate committee and is ready for submission to the university library.

Date

Michael A. Jensen
Chair, Graduate Committee

Accepted for the Department

Michael A. Jensen
Graduate Coordinator

Accepted for the College

Douglas M. Chabries
Dean, College of Engineering and Technology

ABSTRACT

UNITARY SPACE-TIME TRANSMIT DIVERSITY FOR MULTIPLE ANTENNA SELF-INTERFERENCE SUPPRESSION

Adam L. Anderson
Department of Electrical and Computer Engineering
Master of Science

A common practice for government defense agencies and commercial aeronautical companies is to use dual antennas on test flight air vehicles in order to overcome occlusion issues during high-speed telemetric maneuvers. The dual antennas, though never being masked at the same time, unfortunately lead to a drastic increase in nulls in the signal pattern. The result of this interference pattern can be compared to the effect of fading in a multiple-input multiple-output (MIMO) multi-path scattering environment. Confidence in this comparison leads to the use of unitary space-time MIMO codes to overcome the signal self-interference. The possibility and performance of several of these codes will be examined. Such criteria as training for channel estimation, use of shaped offset quadrature phase shift keying (SOQPSK), hardware facility, and data throughput will be compared for each code. A realistic telemetry channel will be derived to increase accuracy of simulated results and conclusions.

ACKNOWLEDGMENTS

At the risk of sounding cliche I would like to thank my wife, Brita, first and foremost at the beginning of this thesis. Not only for direct help (like long hours of editing and reproducing Figure 5.3) but for all she had to put up with as I finished the requirements for my Master's degree. I also acknowledge my two sons, Maxwell and Chase, for bringing me so much joy and having had to go without a father once in a while during my schooling.

I thank, also, my graduate advisor (and employer) Michael Jensen. As I graduate with my Masters, Dr. Jensen will have accumulated over four years as an advisor and friend. He was the first to get me thinking about advanced degrees for which I thank him.

And finally, I am appreciative of The Church of Jesus Christ of Latter-day Saints for providing such great institutions as Brigham Young University. Also, I give acknowledgements to the government sponsors without whom research would be so difficult.

Contents

List of Tables

List of Figures

Chapter 1

Introduction

Air-to-ground telemetry of a variety of data relating to vehicle and pilot status is a common practice during flights of military aircraft. This telemetry is typically accomplished using a wireless link that in many cases, such as during test flights by the United States Air Force, are unidirectional (air-to-ground only). In such cases, maintaining a reliable data link is of high importance.

One key problem encountered in these telemetry links is that during aggressive air-vehicle maneuvering, the transmission from the aircraft-mounted transmit antenna to the receiving ground station can be obstructed or "masked" by the aircraft itself, resulting in loss of the telemetry data. To overcome this problem, two antennas can be mounted on the aircraft at different locations to maintain a high probability that at least one of the antennas will have a strong link to the ground station. Unfortunately, this practice leads to self-interference when neither antenna is masked, resulting once again in data loss. A communication technique is therefore needed that maintains link integrity for all possible aircraft attitudes.

This thesis demonstrates the use of orthogonal transmit diversity schemes to facilitate telemetry transmission from two antennas and to enable communication when either antenna is masked while eliminating the self-interference observed when neither antenna is masked. Specifically, the study will focus on the Alamouti transmit diversity scheme and a differential space-time coding technique. The development includes an intuitive description of the algorithm operation for this application as well as detailed investigations of the algorithm performance in realistic telemetry channels. The algorithms are also extended to the shaped-offset quadrature phase

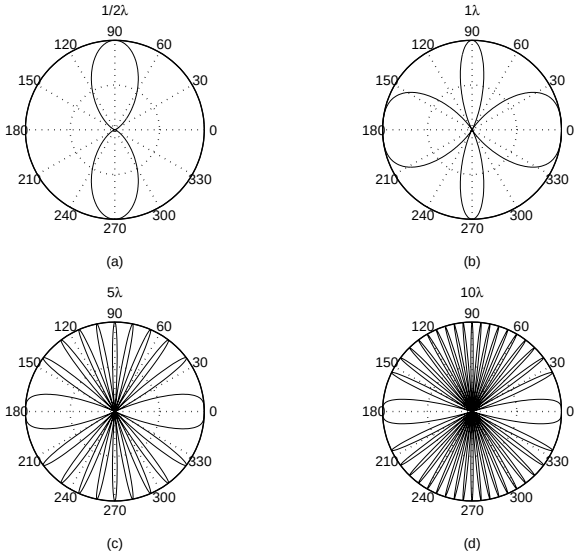

Figure 1.1: Plots (a)-(d) show interference patterns cause by antenna separations of .5, 1, 5, and 10 wavelengths respectively.

shift keying (SOQPSK) modulation proposed for use in future telemetry systems for aeronautical test flights.

1.1 Dual-Antenna Self-Interference

A well known phenomenon of antenna radiation is demonstrated in Figure 1.1; as separation between antenna elements increases the spatial frequency of pattern nulls also increases. As previously mentioned, in order to have a high probability that at least one antenna retains a reliable link during test flight maneuvers the antennas *must* be widely separated (above and below the aircraft for example). This wide separation will lead immediately to a signal pattern similar to Fig. 1.1(d) for the aeronautical telemetry channel. As the aircraft maneuvers, the signal direction to the receiver will pass through these nulls, resulting in frequent signal loss. Figure 1.2 shows the signal level that would result at the receiver if the pattern of Fig. 1.1(d) were rotated at one revolution per second. This power fluctuation is clearly problematic.

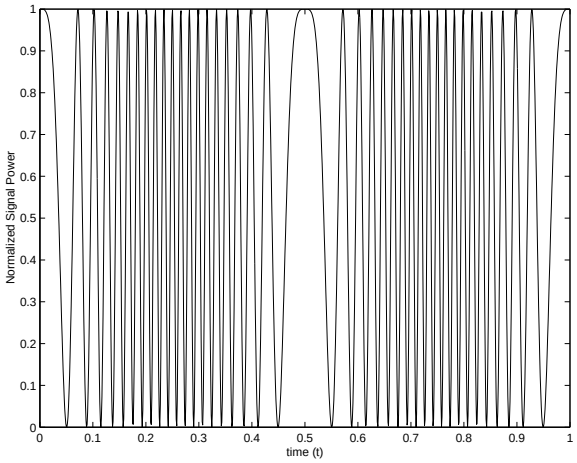

Figure 1.2: Self-interference caused by widely separated antennas is demonstrated by frequent and severe nulls.

1.2 Thesis Contributions

The research focus of this thesis is to provide solutions to the data throughput degradation inherent in widely separated multi-antenna telemetry systems. Several contributions within this arena are outlined, including:

1. Novel use of unitary space-time codes in a non-multipath environment. Specifically, the work will focus on unitary space-time codes [1], [2] often employed to overcome interference caused by multi-path fading environments, to overcome the observed self-interference.

2. Analytical solutions of bit error rate for Alamouti's code and traditional dual-antenna transmission. Analytical expressions for the bit error performance of the traditional transmission scheme as well as Alamouti's code will be derived. These expressions will aid in demonstrating the vast improvement using transmit diversity brings over standard transmission.

3. Functional integration of space-time codes with preexisting hardware. Current

telemetry systems employ SOQPSK transmitters as well as differential bit encoding to increase the spectral efficiency of the system. The offset and memory-introducing nature of these systems makes standard space-time encoding and detection impossible. This thesis explores the creation of a pre-coding block that enables space-time codes to be used at the transmitter as well as novel detection schemes at the receiver.

4. Realistic telemetry channel coefficient calculation and flight path. Finally, a realistic flight channel model will be defined along with telemetric channel coefficient estimation calculation. This channel model will be used extensively for simulation purposes as it affects the real-life situation of non-multipath self-interference.

1.3 Thesis Organization

The remainder of the thesis in organized as follows. In Chapter 2 the traditional transmission scheme will be examined in detail. An explanation of its frailties will be given through analytical representations of error performance as well as graphical visualization of signal pattern interference. Chapters 3 and 4 will present two orthogonal space-time codes used to overcome the effects of interference caused by fading channels - Alamouti's code and differential space-time modulation. These two codes will be compared for optimality for the stated problem. Future telemetry systems will use more advanced technology such as SOQPSK transmitters for overall system enhancement. Chapter 5 explains how space-time codes can be integrated into such systems. Chapter 6 concludes the thesis and presents subjects for future research while Appendix A is a detailed derivation of the aeronautical telemetry channel coefficients.

Chapter 2

Background

2.1 History

As was mentioned in the introduction, during aircraft test flights, aggressive maneuvering can lead to situations where the channel between the aircraft-mounted telemetry antenna and ground station is obstructed by the air vehicle itself. To overcome this problem, a second antenna is commonly placed on the aircraft to ensure at least one of the antennas has a clear, line-of-sight (LOS) path to the ground station. Identical data streams are transmitted simultaneously from each antenna to allow redundancy in the advent of single antenna occlusion.

While this two-antenna transmission approach solves the problem of data outages due to antenna masking, the fact that the antennas must be spaced many wavelengths apart (i.e. situated on different areas of the aircraft) introduces another problem. Specifically, from traditional antenna array theory, it is well known that the composite radiation pattern of two widely separated antennas is characterized by a large number of radiation peaks and nulls. Therefore, in the common situation where neither antenna is masked by the aircraft, vehicle maneuvering leads to frequent signal loss when a pattern null is directed at the ground receiver.

The goal of this chapter is to formulate a model describing the aeronautical telemetry channel and to quantify the error performance of telemetry systems operating in this environment. First, a simple analytical solution for the error rate performance of a model telemetry system is developed for single and dual antenna transmissions. Results from this solution are then compared to those obtained from

simulations based on a channel model for a maneuvering air-vehicle. The results demonstrate the poor performance of these traditional telemetry systems and therefore motivate development of more sophisticated communication schemes.

2.2 Single Antenna Transmission

An analytical expression for the bit error rate (BER) for single-input single-output (SISO) quadrature phase shift keyed (QPSK) systems will now be developed assuming any masking between transmit and received antennas can be ignored. Consider transmission of a symbol, denoted by s, through the channel from the aircraft to the receiver. At the output of the matched filter, the complex baseband received signal can be expressed as

$$r = hs + \eta, \tag{2.1}$$

where h is the complex channel transfer function and η is complex additive white Gaussian noise (AWGN). The received signal energy is

$$E_r = E\{(hs)(hs)^*\} = |h|^2 E_s \tag{2.2}$$

where E_s is the average energy of the transmitted symbol. In a similar manner the complex noise energy can be defined as

$$E\{\eta\eta^*\} = \sigma_\eta^2 = N_0, \tag{2.3}$$

where σ_η^2 represents the total complex noise variance and N_0 is the noise power spectral density [3]. Assume that the channel coefficient is normalized such that $|h|^2 = 1$ and for convenience the total signal-to-noise ratio (SNR) per symbol will be written as $\gamma_s = E_s/N_0$. The probability of a bit error for QPSK signals has been derived previously [3] and is given as

$$p(E) = \mathrm{Q}\left(\sqrt{\frac{2E_b}{N_0}}\right) \tag{2.4}$$

$$Q(x) = \frac{1}{2}\mathrm{erfc}\left(\frac{x}{\sqrt{2}}\right) \tag{2.5}$$

where $\mathrm{erfc}(\cdot)$ represents the complementary error function and $E_s = 2E_b$ for QPSK signals. Eq. (2.4) serves as a baseline to which the performance of alternate transmission schemes can be compared.

2.3 Dual Antenna Transmission

Dual-antenna transmission will in general be referred to as a multiple-input single-ouput (MISO) scheme. In traditional dual-antenna transmission the same data stream is fed to each transmit antenna. However, due to the different locations of the two transmit antennas, the channel coefficients h_1 and h_2 differ for the two streams. The received signal for this case can be expressed as

$$r = h_1\frac{s}{\sqrt{2}} + h_2\frac{s}{\sqrt{2}} + \eta = (h_1 + h_2)\frac{s}{\sqrt{2}} + \eta, \tag{2.6}$$

where η is complex AGWN and the $\frac{1}{\sqrt{2}}$ term comes from the fact that transmit power is split equally between both antennas. The received signal energy is expressed as

$$\begin{aligned} E_s &= \mathrm{E}\{(h_1 + h_2)\frac{s}{\sqrt{2}}(h_1 + h_2)^*\frac{s^*}{\sqrt{2}}\} \\ &= \mathrm{E}\{|h_1 + h_2|^2\}E\{|\frac{s}{\sqrt{2}}|^2\} \\ &= \frac{1}{2}|h_1 + h_2|^2 E_s \end{aligned} \tag{2.7}$$

while the received noise energy remains

$$E\{\eta\eta^*\} = \sigma_\eta^2 = N_0. \tag{2.8}$$

Using Eqs. (2.7) and (2.8) the effective SNR per symbol at the receiver can be defined as

$$\gamma_s = \frac{\frac{1}{2}|h_1(\theta,\phi) + h_2(\theta,\phi)|^2 E_s}{N_0}. \tag{2.9}$$

The channel coefficients are in general functions of the angles (θ, ϕ) describing the direction of the receiver in the coordinate frame of the aircraft. A problem associated with traditional dual-antenna transmission is immediately observed in Eq. (2.9). As h_1 and h_2 approach the state of being equal in magnitude and opposite in phase the term $|h_1 + h_2|$ approaches zero, decreasing the SNR at the receiver and increasing the probability of error.

Using Eq. (2.4) with Eq. (2.9) along with channel dependence on (θ, ϕ), the probability of error for a given aircraft attitude is

$$\begin{aligned} p(E|\theta,\phi) &= \mathrm{Q}\left(\sqrt{\frac{2E_b}{N_0}\frac{1}{2}|h_1(\theta,\phi)+h_2(\theta,\phi)|^2}\right) \\ &= \mathrm{Q}\left(\sqrt{\frac{E_b}{N_0}|h_1(\theta,\phi)+h_2(\theta,\phi)|^2}\right). \end{aligned} \tag{2.10}$$

A simple demonstration of the performance of this communication strategy can be obtained by fixing $\theta = \pi/2$ and assuming that ϕ is uniformly distributed over a maneuver, or

$$p_\phi(\phi) = \begin{cases} \frac{1}{2\pi} & 0 \le \phi \le 2\pi \\ 0 & \text{otherwise.} \end{cases} \tag{2.11}$$

Using Eqs. (2.10) and (2.11) the probability of error simplifies to

$$\begin{aligned} p(E) &= \int_0^{2\pi}\int_0^{\pi} p(E|\theta,\phi)p(\theta)p(\phi)\mathrm{d}\theta\mathrm{d}\phi \\ &= \frac{1}{2\pi}\int_0^{2\pi} \mathrm{Q}\left(\sqrt{\frac{E_b}{N_0}\left|h_1\left(\frac{\pi}{2},\phi\right)+h_2\left(\frac{\pi}{2},\phi\right)\right|^2}\right)\mathrm{d}\phi. \end{aligned} \tag{2.12}$$

This integral must be computed numerically. The results from this anaylsis can be directly compared with those from Eq. (2.4) to demonstrate the impact of the signal nulls observed in a communication system using widely separated antennas.

Further insights into problems associated with traditional MISO scenarios can be seen by examining the signal response. Assume for now a simplified scenario where the two antennas are placed some distance d apart along the x-axis, and that the receiver lies in the x-y plane at an angle ϕ from the x-axis. In this case, the received signal can be expressed as (compare to Eq. (2.6))

$$\begin{aligned} r &= e^{j\frac{kd\cos\phi}{2}}\frac{s}{\sqrt{2}} + e^{-j\frac{kd\cos\phi}{2}}\frac{s}{\sqrt{2}} + \eta \\ &= \frac{2}{\sqrt{2}}\cos\left(\frac{kd\cos\phi}{2}\right)s + \eta. \end{aligned} \tag{2.13}$$

Figure 2.1 shows the received signal pattern as a function of ϕ assuming unity power per symbol and a spacing of 10λ between the antennas. Notice the extreme and frequent nulls that occur as the aircraft attitude changes. This rapid variation causes data loss when the aircraft is situated such that a null is directed at the receiver.

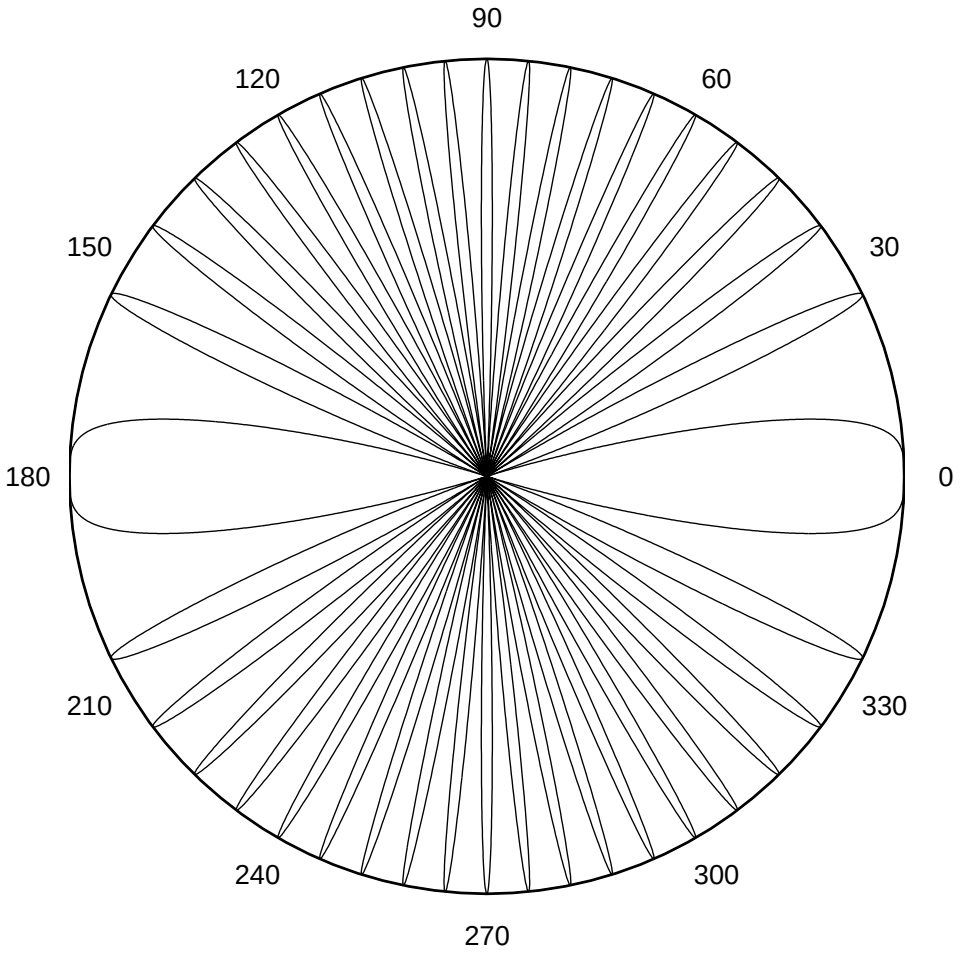

Figure 2.1: Received signal versus angle ϕ for two transmit antennas spaced 10λ apart.

2.4 Simulation Results

For simulation purposes a performance curve can be generated by first assuming that the total channel phase, $\phi_h = \arg\{h_1 + h_2\}$, has been tracked and estimates are available at the receiver. The received signal r from Eq. (2.6) can then be transformed to the following symbol estimate

$$\tilde{s} = e^{-j\phi_h} r = \text{mag}\{h_1 + h_2\} \frac{s}{\sqrt{2}} + e^{-j\phi_h} \eta \tag{2.14}$$

which is sent to a maximum likelihood detector. The analytical solution of the SISO BER from Eq. (2.4) is a well tested and often used expression. Simulating the MISO, traditional transmission scenario in the telemetry channel is important to confirm and give confidence in the results of the analytical approach. For this simulation a simple airborne maneveur was performed with transmit and receive antennas situated as described in Appendix A. A random data stream of 2×10^5 bits was produced and encoded using standard QPSK modulation symbols. The same symbols were sent out each antenna at exactly the same instance in time where any differential timing delay between the two antennas was ignored. Each received matched filter output was decoded per Eq. (2.14).

Figure 2.2 shows the BER performance for traditional dual-antenna transmission resulting from using the analytical and simulated models. In Figure 2.3 an enlarged portion of the plot (around 5dB) is displayed demonstrating the accuracy of the analytical solution. Notice the non-standard scaling on the y-axis. The discrepency between the two plots is due to the finite number of symbols transmitted. The difference is small enough that the analytical solution can be used with confidence and for brevity in simulation.

Further, a comparison of the SISO and MISO BERs are shown in Figure 2.4. In addition to the performance curve for SISO transmission ignoring antenna masking, a more realistic plot is shown where aircraft motion was such that 20% of the time the transmit antenna was masked resulting in total signal loss. Several interesting observations are readily apparent by comparing these three curves. First, the performance of the traditional dual-antenna transmission scheme is very poor.

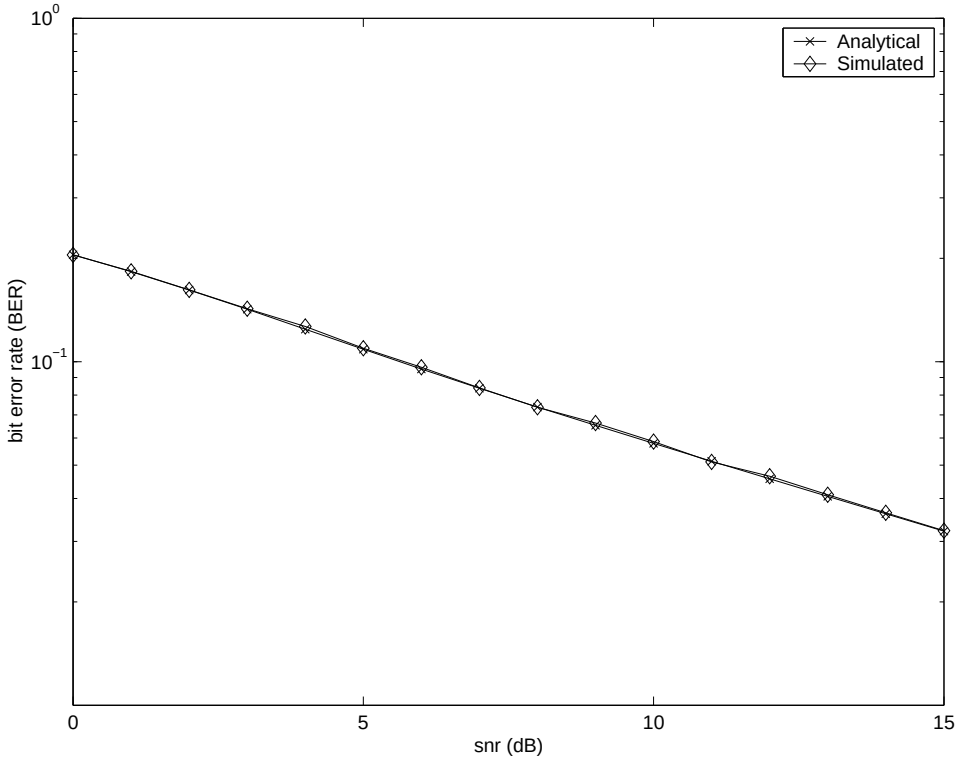

Figure 2.2: Bit error rates for dual-antenna transmission as produced by the analytical and simulated models.

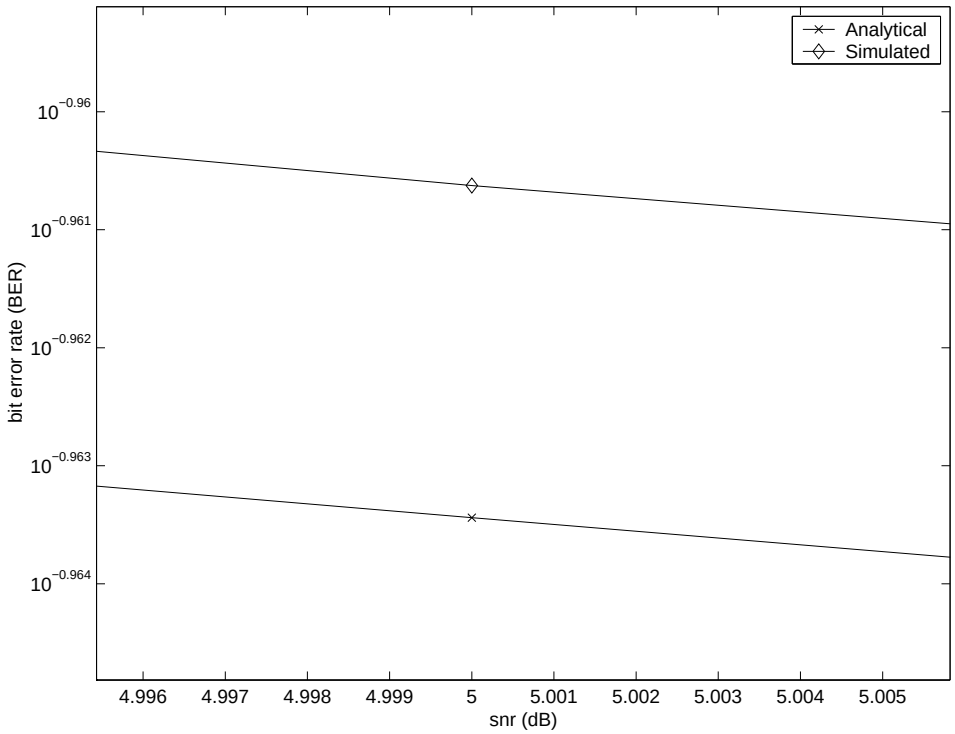

Figure 2.3: Bit error rate for no transmit diversity as produced by the analytical and simulated models. The plot has been enlarged around 5dB.

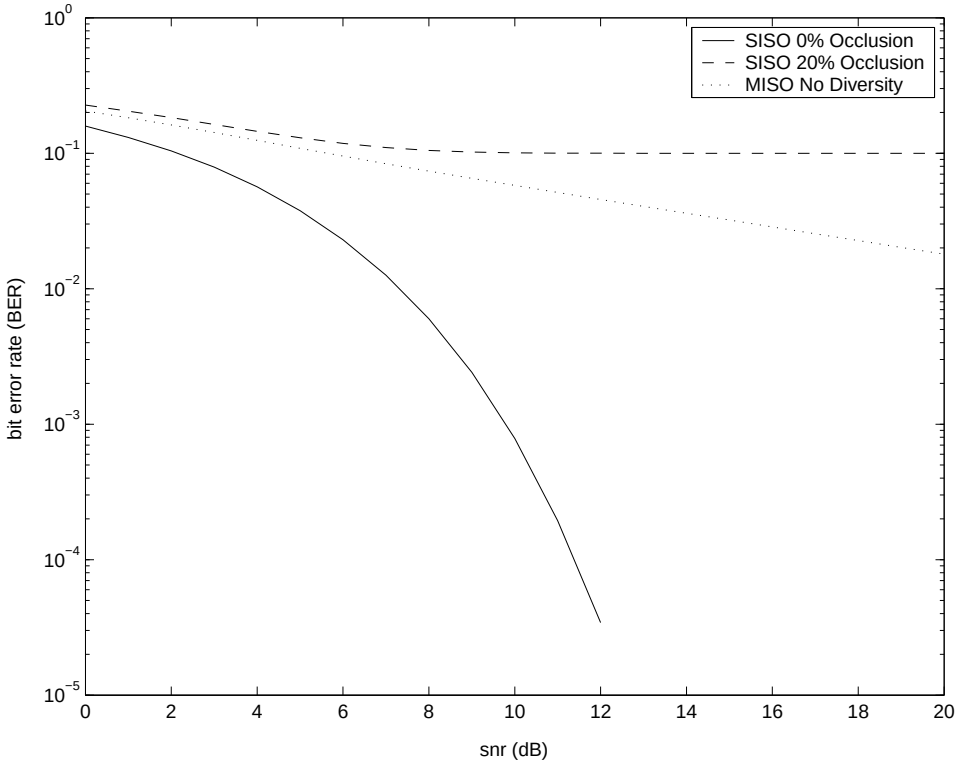

Figure 2.4: Symbol error rates (BER) for SISO transmission with and without occlusion. Also shown is dual antenna transmission with no transmit diversity.

In fact, this performance is very similar to a telemetry channel experiencing extreme multipath fading interference. Second, though obviously poor, using dual-antennas does perform well in that it overcomes previously stated issues caused by aircraft occlusion.

Chapter 3

Alamouti's Space-Time Code

In [1] Alamouti presented a simple and effective transmit encoding scheme to overcome multipath distortion caused by fading. This strategy was specifically designed for communication systems using two transmit and M receive antennas and consists of three basic operations:

1. Proper encoding of symbols at the transmitter
2. Signal combination at the receiver
3. Maximum likelihood signal decision

As will be seen, an important aspect of Alamouti encoding is that nearly all of the computational burden is placed at the receiver. This is appropriate as in many telemetry systems (specifically the ones addressed in this thesis) size constraints may preclude excessive equipment on the aircraft.

This chapter explores Alamouti's space-time code and its functionality in the telemetry channel. Its superiority over traditional transmission will be demonstrated through performance simulations, and an explanation of its operation in the dual-antenna telemetry channel will be provided. Additional issues associated with Alamouti's scheme, such as channel coefficient estimation, will also be addressed.

3.1 Alamouti Transmission

An Alamouti transmission period spans two consecutive symbol periods, n and $n+1$, with information bearing symbols denoted as s_n and s_{n+1}. During the

Table 3.1: Alamouti's encoding scheme for two transmit antennas.

symbol time	antenna 1	antenna 2
n	s_n	s_{n+1}
n + 1	$-s^*_{n+1}$	s^*_n

n^{th} symbol time antenna 1 transmits s_n while antenna 2 simultaneously transmits s_{n+1}. During the second half of an Alamouti period antenna 1 will transmit $-s^*_{n+1}$ with antenna 2 transmitting s^*_n. Table 3.1 shows the manner in which symbols are encoded using Alamouti's scheme.

Assuming channel coefficients remain constant over the Alamouti period, two receiver matched filter outputs for these two symbol times are given as

$$r_n = h_1 \frac{s_n}{\sqrt{2}} + h_2 \frac{s_{n+1}}{\sqrt{2}} + \eta_n \tag{3.1}$$

$$r_{n+1} = -h_1 \frac{s^*_{n+1}}{\sqrt{2}} + h_2 \frac{s^*_n}{\sqrt{2}} + \eta^*_{n+1} \tag{3.2}$$

where the channel functions h_1 and h_2 as well as the noise η_n are defined in Chapter 2. Taking the conjugate of Eq. (3.2) allows the received signal to be written in matrix-vector form as

$$\begin{aligned} \mathbf{r}_n &= \begin{bmatrix} r_n \\ r^*_{n+1} \end{bmatrix} \\ &= \frac{1}{\sqrt{2}} \begin{bmatrix} h_1 & h_2 \\ h^*_2 & -h^*_1 \end{bmatrix} \begin{bmatrix} s_n \\ s_{n+1} \end{bmatrix} + \begin{bmatrix} \eta_n \\ \eta_{n+1} \end{bmatrix} \\ &= \frac{1}{\sqrt{2}} \mathbf{H} \mathbf{s_n} + \boldsymbol{\eta}_n. \end{aligned} \tag{3.3}$$

The ingenuity behind Alamouti's scheme can be seen by evaluating the following product

$$\begin{aligned}\mathbf{H}^{\dagger}\mathbf{H} &= \begin{bmatrix} h_1 & h_2 \\ h_2^* & -h_1^* \end{bmatrix} \begin{bmatrix} h_1^* & h_2 \\ h_2^* & -h_1 \end{bmatrix} \\ &= \begin{bmatrix} |h_1|^2 + |h_2|^2 & h_1^* h_2 - h_1^* h_2 \\ h_1 h_2^* - h_1 h_2^* & |h_1|^2 + |h_2|^2 \end{bmatrix} \\ &= (|h_1|^2 + |h_2|^2)\mathbf{I}, \end{aligned} \tag{3.4}$$

were $\{\cdot\}^{\dagger}$ denotes a conjugate transpose operation. Therefore, H is an orthogonal matrix. This orthogonality allows estimation of the transmitted vector with

$$\tilde{\mathbf{s}} = \mathbf{H}^{\dagger}\mathbf{r} = \frac{1}{\sqrt{2}}(|h_1|^2 + |h_2|^2)\mathbf{s} + \mathbf{H}^{\dagger}\boldsymbol{\eta}. \tag{3.5}$$

Detection is done by finding the minimum Euclidean distance between symbols and symbol estimates.

The received signal SNR can be computed starting with explicit expressions for symbol estimates from Eq. (3.5)

$$\tilde{s}_1 = (|h_1|^2 + |h_2|^2)\frac{s_1}{\sqrt{2}} + h_1^*\eta_1 + h_2\eta_2^* \tag{3.6}$$

$$\tilde{s}_2 = (|h_1|^2 + |h_2|^2)\frac{s_2}{\sqrt{2}} - h_1\eta_2^* + h_2^*\eta_1. \tag{3.7}$$

Using (3.6), the received signal energy per symbol ($E_{r,1}$) for the first symbol estimate $\tilde{s}_1$ is

$$E_{r,1} = \frac{1}{2}\mathrm{E}\{(|h_1|^2 + |h_2|^2)^2 s_1 s_1^*\} = \frac{1}{2}(|h_1|^2 + |h_2|^2)^2 E_{s_1} \tag{3.8}$$

while the received noise energy ($N_{0,1}$) for $\tilde{s}_1$ is

$$\begin{aligned} N_{0,1} &= \mathrm{E}\{(h_1^*\eta_1 + h_2\eta_2)(h_1\eta_1^* + h_2^*\eta_2^*)\} \\ &= |h_1|^2\mathrm{E}\{\eta_1\eta_1^*\} + |h_2|^2\mathrm{E}\{\eta_2\eta_2^*\} \\ &= N_0(|h_1|^2 + |h_2|^2) \end{aligned} \tag{3.9}$$

where $\mathrm{E}\{\eta_1\eta_2\} = 0$ and $N_0 = \sigma_{\eta_1}^2 = \sigma_{\eta_2}^2$ as discussed in Chapter 2. A similar treatment is performed to find signal and noise energies for $\tilde{s}_2$:

$$E_{r,2} = \frac{1}{2}\mathrm{E}\{(|h_1|^2 + |h_2|^2)^2 s_2 s_2^*\} = \frac{1}{2}(|h_1|^2 + |h_2|^2)^2 E_{s_2} \tag{3.10}$$

and

$$\begin{aligned} N_{0,2} &= \mathrm{E}\{(h_2^*\eta_1 - h_1\eta_2)(h_2\eta_1^* - h_1^*\eta_2^*)\} \\ &= |h_2|^2\mathrm{E}\{\eta_1\eta_1^*\} + |h_1|^2\mathrm{E}\{\eta_2\eta_2^*\} \\ &= N_0(|h_1|^2 + |h_2|^2). \end{aligned} \tag{3.11}$$

Assuming $E_s = E_{s_1} = E_{s_2}$ the received symbol SNR can the be expressed as

$$\gamma_s = \frac{E_{r,1}}{N_{0,1}} = \frac{E_{r,2}}{N_{0,2}} = \frac{E_s}{N_0}\frac{(|h_1|^2 + |h_2|^2)}{2}. \tag{3.12}$$

Recall that with traditional MISO transmission, the term $(|h_1|^2 + |h_2|^2)$ is replaced with $(|h_1 + h_2|^2)$ (see Eq. (2.14)) which implies that the functions h_1 and h_2 can destructively interfere for certain aircraft attitudes. Because the form in Eq. (3.12) adds the magnitudes of the transfer functions, this interference does not occur when Alamouti's scheme is employed. Furthermore, if one of the transfer functions goes to zero due to obstruction by the air vehicle, the only degradation is a reduction in the received signal SNR (by approximately 3dB). Therefore, Alamouti's code appears to provide robustness to antenna masking without introducing the destructive self-interference associated with traditional MISO transmission.

Using the framework from Chapter 2 it is possible to formulate the probability of a bit error for the Alamouti scheme. Substituting Eq. (3.12) into Eq. (2.4) the probability of error conditioned on a specific aircraft attitude (angles to the receiver) becomes

$$\begin{aligned} P(\mathcal{E}|\theta,\phi) &= \mathrm{Q}\left(\sqrt{\gamma_s}\right) \\ &= \mathrm{Q}\left(\sqrt{\frac{E_s}{2N_0}(|h_1(\theta,\phi)|^2 + |h_2(\theta,\phi)|^2)}\right). \end{aligned} \tag{3.13}$$

As was done for traditional dual-antenna transmission, a simple demonstration of the performance of this communication strategy can be obtained by fixing $\theta = \pi/2$ and assuming that ϕ is uniformly distributed over a maneuver, or

$$p_\phi(\phi) = \begin{cases} \frac{1}{2\pi} & 0 \le \phi \le 2\pi \\ 0 & \text{otherwise.} \end{cases} \tag{3.14}$$

Using Eqs. (3.13) and (3.14) the probability of error simplifies to

$$\begin{aligned} P(\mathcal{E}) &= \int_0^{2\pi}\int_0^{\pi} P(\mathcal{E}|\theta,\phi)p_\theta(\theta)p_\phi(\phi)\mathrm{d}\theta\mathrm{d}\phi \\ &= \frac{1}{2\pi}\int_0^{2\pi} \mathrm{Q}\left(\sqrt{\frac{E_b}{N_0}\left|h_1\left(\frac{\pi}{2},\phi\right)\right|^2 + \left|h_2\left(\frac{\pi}{2},\phi\right)\right|^2}\right)\mathrm{d}\phi. \end{aligned} \tag{3.15}$$

This integral must be evaluated numerically.

A graphical approach can be taken to provide further intuitive insights into the operation of Alamouti's code in dual-antenna telemetry transmission. Imagine a scenario where two QPSK symbols desired to be transmitted during an Alamouti period are (for simplicity) s_a and s_a. As per Alamouti encoding these two symbols are transmitted during the first symbol time from their respective antennas with $-s_a^*$ and s_a^* transmitted during the second symbol time. Similar expressions to Eq. (2.13) for the received signal strength as a function of angle can be written for the consecutive received signals over the Alamouti period

$$\begin{aligned} \rho_n(\phi) &= \sqrt{2}\cos\left(\frac{kd\cos\phi}{2}\right)s_a \\ \rho_{n+1}(\phi) &= -\mathrm{j}\sqrt{2}\sin\left(\frac{kd\cos\phi}{2}\right)s_a^*. \end{aligned} \tag{3.16}$$

The magnitudes of these functions versus ϕ are displayed in Figures 3.1 and 3.2. These plots suggest that if the aircraft is situated such that a null is directed at the receiver for one symbol period, a peak will be directed at the receiver during the next symbol period. Stated another way, the sum pattern over an Alamouti period is $|\rho_n(\phi)|^2 + |\rho_{n+1}(\phi)|^2 = 4$, which implies omni-directional radiation.

3.2 Simulation Results

It has been demonstrated both qualitatively and quantitatively how the Alamouti scheme overcomes the poor performance observed in traditional dual-antenna transmission. It is now instructive to further quantify the performance gains through computational simulations. The telemetry channel model used to simulate the performance of the traditional MISO transmission was used for these simulations as well (see Appendix A). Random data comprised of 2×10^5 bits was converted into QPSK

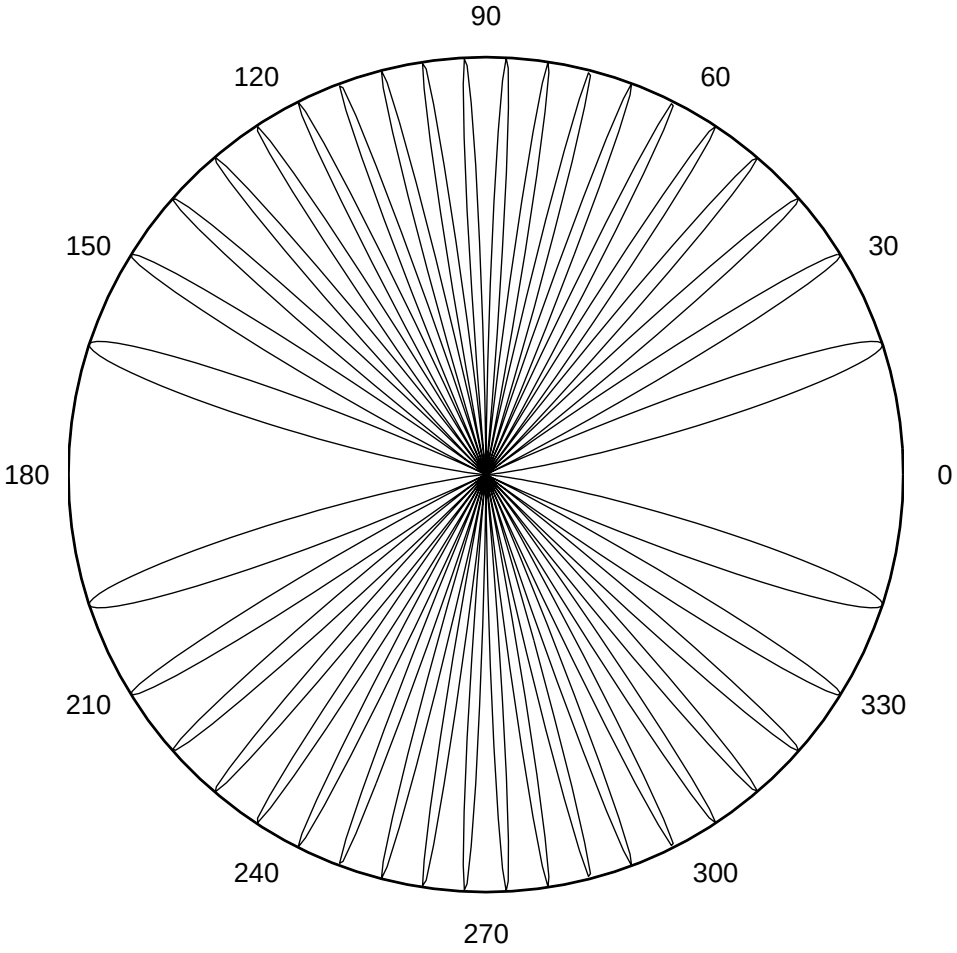

Figure 3.1: Radiation pattern from first transmission time using Alamouti's code.

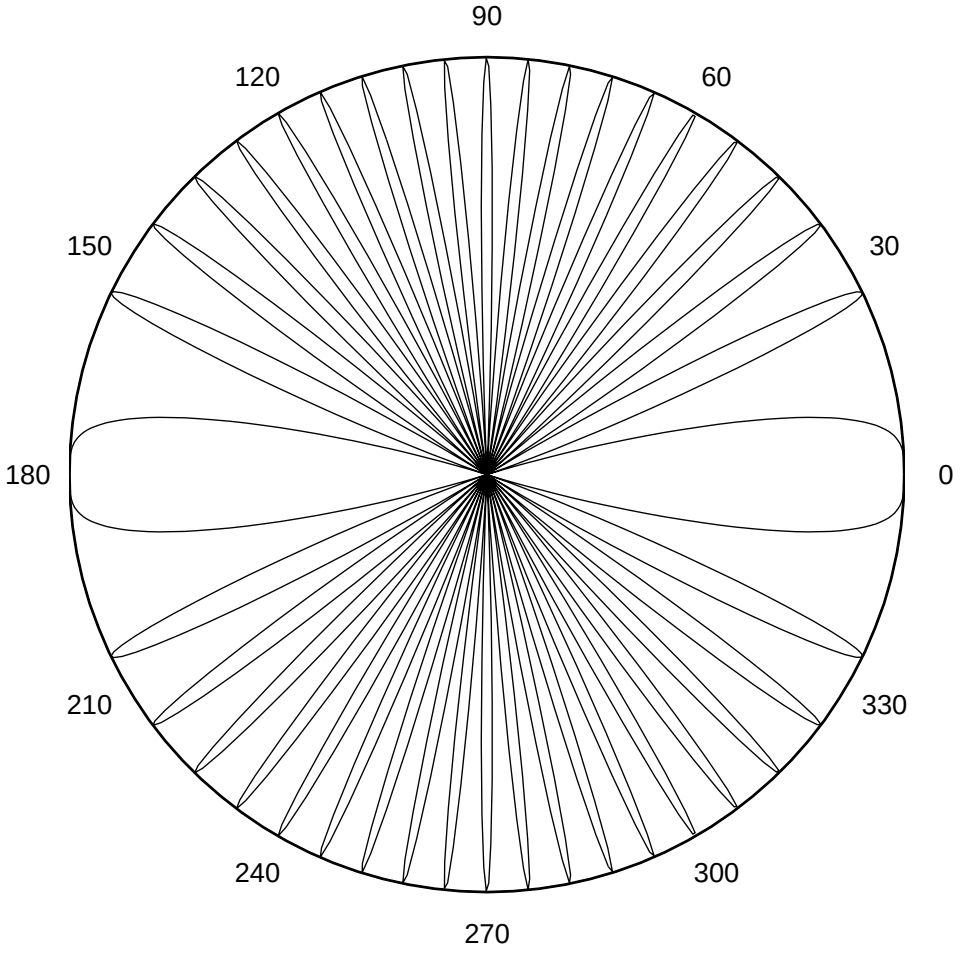

Figure 3.2: Radiation pattern from second transmission time using Alamouti's code.

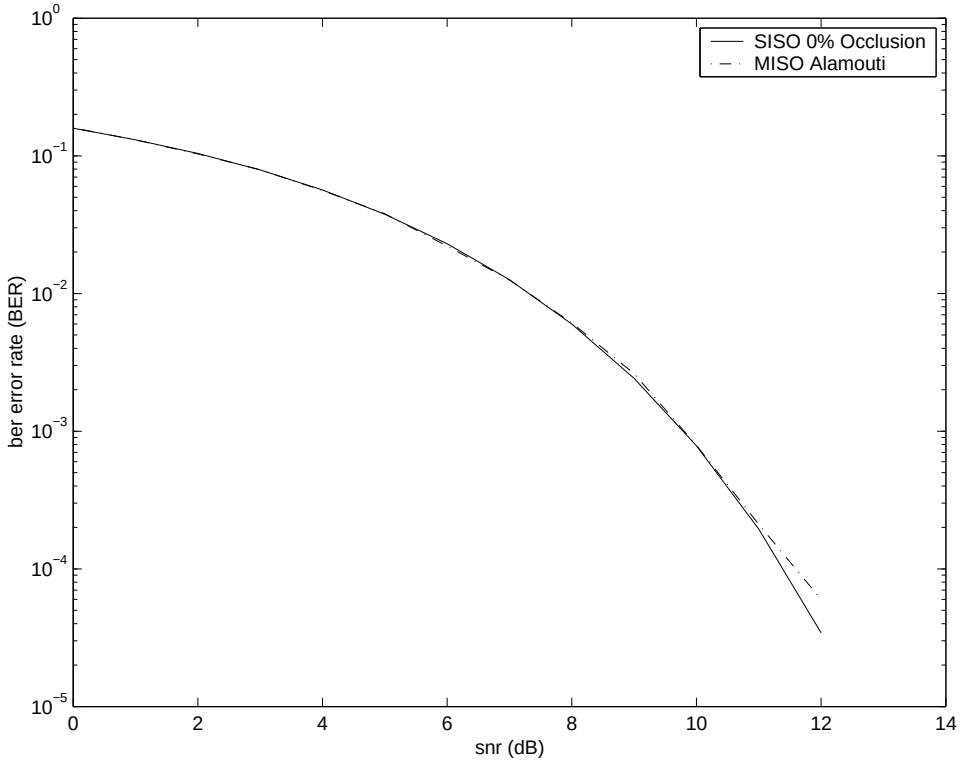

Figure 3.3: Alamouti's code produces the same BER as the unobstructed SISO transmission.

symbols using standard Gray encoding and then transmitted via Alamouti's scheme. After passing through the channel, complex AWGN was added at the receiver. Complex baseband samples were taken each symbol period and decoded according to Eq. (3.5) with perfect channel state information (CSI) assumed at the receiver.

Figure 3.3 shows the BER performance of Alamouti's code in the telemetry channel as well as the non-obstructed SISO transmission. The error performance of Alamouti's code exactly achieves the error performance of non-obstructed SISO transmission. It is instructional to reiterate here that the SISO curve was produced assuming a perfect LOS channel while the Alamouti simulation experienced the frequent pattern nulls explained in Chapter 2. Obviously, Alamouti's code overcomes this self-interference and demonstrates an effective omni-directional radiation pattern as was suggested previously.

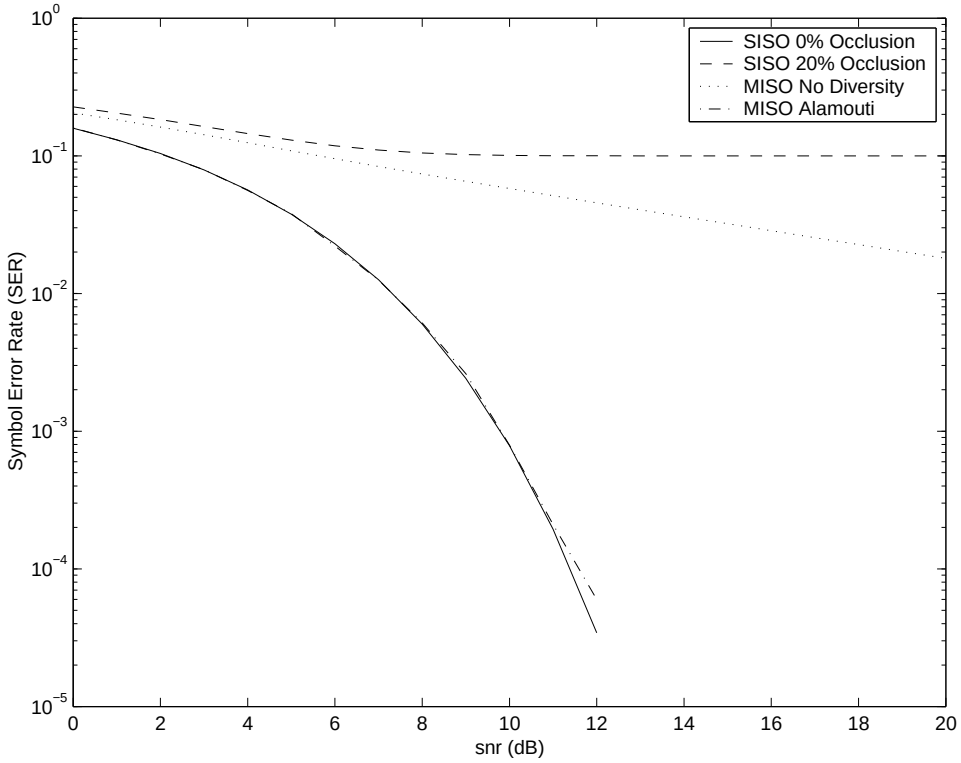

Figure 3.4: Performance rates of various transmission schemes.

Figure 3.4 shows the performance of the three transmission schemes examined thus far: standard SISO, MISO with no transmit diversity, and finally MISO using Alamouti's transmit diversity. As is readily apparent, Alamouti's scheme not only overcomes the problem of a non-multipath self-interference channel but also is relatively impervious to antenna occlusion.

It may seem astounding at first glance that Alamouti's scheme is so insusceptible to antenna masking and inherent antenna self-interference problems. A quick mathematical derivation will show its functionality. Assume that one antenna is masked such that $h_1 = 0$, resulting in complete signal loss from that antenna. For this situation Eq. (3.5), the received estimate, becomes

$$\tilde{\mathbf{s}} = \mathbf{H}^{\dagger}\mathbf{r} = \frac{1}{\sqrt{2}}|h_2|^2\mathbf{s} + \mathbf{H}^{\dagger}\boldsymbol{\eta} \tag{3.17}$$

which takes a 3dB hit in performance, but the signal vector $\mathbf{s}$ is obviously still detectable.

3.3 Channel Estimation

The analytical solution of BER curves for Alamouti's code ignores imperfections in channel estimates. In order to assess performance in live operational situations, channel estimates for realistic maneuvers must be taken into account - motivating the use of the simulation model as discussed in Chapter 2. The analytical model was created under the assumption that perfect channel knowledge was available at the receiver. Such an assumption is not valid and indeed impossible. Channel estimates can be realized but an *exact* channel knowledge is impossible, thus the previous results from the analytical solutions suggest a lower bound on error rates.

This section will discuss maximum likelihood channel coefficient estimation and its affect on error performance for Alamouti's code.

3.3.1 Maximum Likelihood Channel Estimation

To illustrate the impact of channel estimation on the performance of a telemetry link employing Alamouti's signaling, we present a simple channel estimation technique. In this approach, a block of N training symbols are transmitted over the channel at some frequency which will be represented as a fraction T of the total time that was spent training.

Assuming the channel estimates do not change significantly over a training period, the matched filter outputs over the training block can then be expressed as

$$[y_1\ y_2\ \ldots\ y_N] = [h_1\ h_2][s_1\ -s_2^*\ \ldots\ -s_N^*] + [\eta_1\ \eta_2\ \ldots\ \eta_N] \tag{3.18}$$

which can be written in matrix form as

$$\mathbf{Y} = \mathbf{HS} + \mathbf{Z}. \tag{3.19}$$

Since the noise samples η_n are independent and identically distributed Gaussian random variables and the training symbols $\mathbf{S}$ are known at the receiver, the maximum

likelihood estimate of the channel is

$$\hat{\mathbf{H}} = [\hat{h}_1 \ \hat{h}_2] = \mathbf{Y}[\mathbf{S}]^{\dagger} \tag{3.20}$$

where $[\cdot]^{\dagger}$ denotes pseudo-inverse. Note, in order for $\mathbf{H}$ to be fully determined there must exist the criterion, $N \geq N_t$, or more training symbols than number of antennas.

3.3.2 BER with Channel Estimation

Accurate channel knowledge is requisite for accurate symbol estimates using Alamouti's code. The maximum likelihood channel estimator allows two degrees of freedom in increasing the accuracy of channel knowledge

1. The fraction of time T spent training
2. The number of symbols N sent per train

Increasing the frequency of training will allow for better CSI as the current channel coefficient estimates will have less available time to go out of date before new estimates are received. Increasing the number of training symbols will allow for more accurate estimates of $\hat{h}_1$ and $\hat{h}_2$. We need to avoid the temptation, though, of spending too much symbol time training and neglecting the transmission of actual data. Ideally, an optimal balance between increasing CSI (via training frequency and training length) and BER performance (better CSI implies better BER) can be found.

Figure 3.5 shows the BER performance of Alamouti's code versus frequency of time training and number of training symbols. These plots were produced by using the simulation model at a fixed SNR of 13dB and no longer assuming perfect CSI. The prescribed maximum likelihood channel estimation algorithm was included in the simulated model with the training variables N and T swept as shown by the x axes.

Similar results are demonstrated between these two optimizing variables. Both reach a point where further increase does not return equal error performance benefits. These points suggest ideal operating values in a live environment. From the

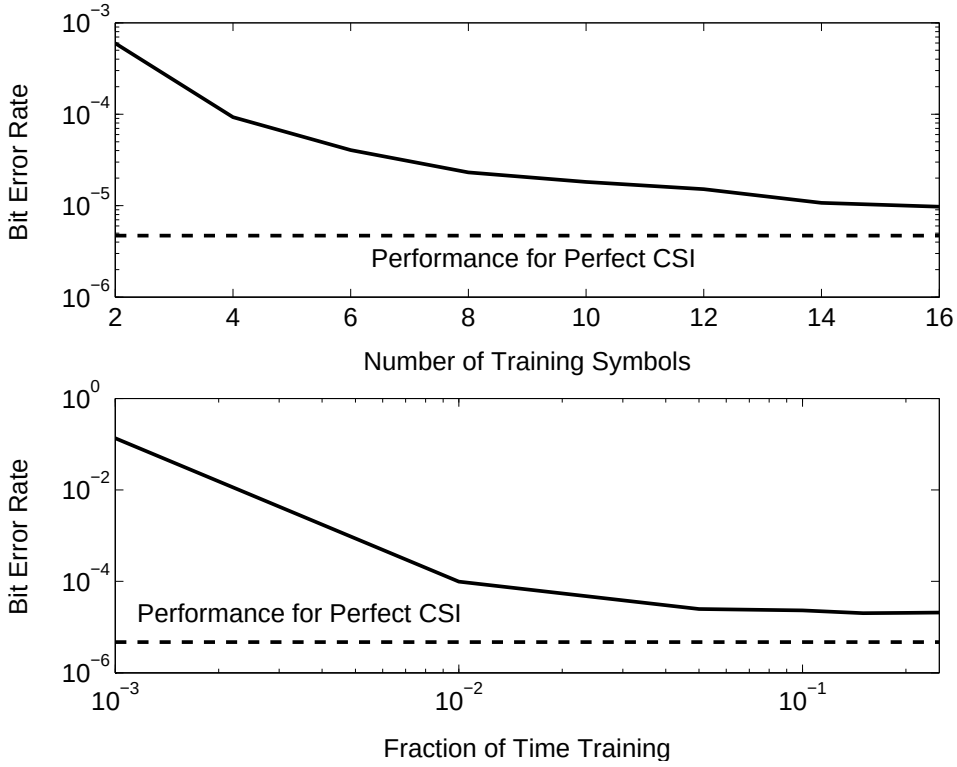

Figure 3.5: Performance response curves as a function of number of training symbols and fraction of time spent training.

simulation results training 1% of the time using 8 training symbols appears to produce sufficiently accurate CSI while not wasting excessive time training. For different operation powers, similar plots could be created and values chosen accordingly.

3.4 Conclusion

Alamouti's code has been show to be an effective coding strategy in overcoming antenna self-interference as well as antenna masking. Analytical solutions for error performance curves have been derived as well as intuitive graphical representations of radiation patterns produced by Alamouti's scheme. A more realistic performance has been demonstrated by the need of channel knowledge at the receiver via a maximum likelihood channel coefficient estimator. A systematic approach was presented in choosing optimal values of number or training symbols and fraction of time training. This need for CSI may appear burdensome, thus motivating the use of space-time codes that do not require channel estimates. These will be presented in the next chapter.

Chapter 4

Differential Space-Time Codes

Thus far this thesis has demonstrated the advantages of using orthogonal space-time codes (specifically Alamouti's scheme) in overcoming the masking and self-interference inherent in MISO telemetry systems. Chapter 3 has shown that one difficulty associated with Alamouti's code is the need for accurate channel state information (CSI) at the receiver. In many situations, however, obtaining an accurate CSI may be impractical and even impossible. For example, consider the telemetry channel. A high speed (exceeding 700 mph) air vehicle performing an exceptionally vigorous maneuver while transmitting at a relatively low data rate ($<$ 2 Mbs) will experience large changes in channel coefficients within relatively few symbol times. Such a rapidly varying channel may cause CSI to quickly become out of date, causing performance degradation through both bit errors and cost of frequent training for channel estimation. In such situations, a space-time code that does not require *any* CSI becomes appealing.

For SISO transmission, symbol detection without the need of CSI can be achieved through such modulation schemes as differential phase shift keying (DPSK). Finding an extension to DPSK for multiple input antenna systems is inherently advantageous for MIMO communication. In [2] Brian L. Hughes presented a systematic approach to differential space-time modulation (DSTM) using cyclic group codes for multiple antenna systems. DSTM exploits multiple antenna channels much like Alamouti modulation, but has the additional advantage of not requiring any channel knowledge at the receiver.

In this chapter a general approach to DSTM using cyclic group block codes will be reviewed. The performance of DSTM in overcoming the self-interference addressed in this thesis will be tested via simulation in the telemetry channel model. Comparisons, specifically pros and cons, between this code and Alamouti's code will also be presented.

4.1 DSTM Transmission

Consider a MISO system with t transmit antennas. Hughes' general approach to differential encoding commences by mapping information bearing bits to unitary matrix groups. Let the group $\mathcal{G} = \{\mathbf{G}_1, \ldots, \mathbf{G}_N\}$ where members of $\mathcal{G}$ are defined by

$$\mathbf{G}_i^\dagger \mathbf{G}_i = \mathbf{G}_i \mathbf{G}_i^\dagger = I \quad \forall\ \mathbf{G}_i \in \mathcal{G} \tag{4.1}$$

and $\{\cdot\}^\dagger$ denotes conjugate transpose. With the group thus defined, and assuming a simple bit-to-matrix mapping, the rate for DSTM using group codes [2] is

$$R = \frac{1}{t}\log_2(N) \text{ b/s/Hz} \tag{4.2}$$

where N is the number of elements in $\mathcal{G}$. As an example of a functional group code, Hughes suggested using the algebraic quaternion group consisting of the matrices

$$\mathcal{G} = \left\{ \pm \begin{bmatrix} 1 & 0 \\ 0 & 1 \end{bmatrix}, \pm \begin{bmatrix} j & 0 \\ 0 & -j \end{bmatrix}, \pm \begin{bmatrix} 0 & -1 \\ 1 & 0 \end{bmatrix}, \pm \begin{bmatrix} 0 & j \\ j & 0 \end{bmatrix} \right\}. \tag{4.3}$$

When used in space-time coding , this group is named the quaternion code. Using Eq. (4.2), the quaternion code is shown to transmit at a rate of $R = 1.5$.

The central idea behind DSTM is that the matrix group codes can be differentially encoded much like symbols in a DPSK modulator. In order to send a block $\mathbf{G}_k$, the *standard encoding equation* is

$$\mathbf{C}_k = \mathbf{C}_{k-1}\mathbf{G}_k\ ,\ k = 1, \ldots, K \tag{4.4}$$

where $\mathbf{G}_k$ represents data bits mapped from group $\mathcal{G}$ and $\mathbf{C}_k$ is the encoded block that is actually transmitted at time k. $\mathbf{C}_0$ is an initialization matrix that is not used

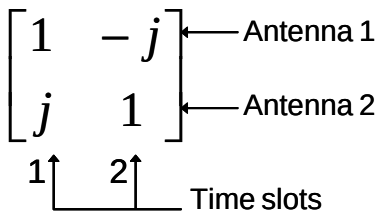

Figure 4.1: Time and space mapping of the matrix elements for differentially encoded blocks.

to transmit data and can be any $t \times t$ matrix that satisfies $\mathbf{C}_0\mathbf{C}_0^\dagger = tI$. For the quaternion code we will use the initial matrix

$$\mathbf{C}_0 = \begin{bmatrix} 1 & -1 \\ 1 & 1 \end{bmatrix}, \tag{4.5}$$

which forces all transmitted matrices C_k to contain element values in the QPSK constellation $\{1, -1, \text{j}, \text{-j}\}$. Figure 4.1 shows how the elements of the encoded blocks C_k are interpreted in space and time. The group structure of $\mathcal{G}$ ensures that for all transmitted blocks, $C_k \in C_0\mathcal{G}$.

After encoding and transmission, received blocks can be expressed as

$$\mathbf{Y}_k = \mathbf{H}\mathbf{C}_k + \mathbf{N}_k \ , \ k = 1, \ldots, K \tag{4.6}$$

where $\mathbf{H}$ is the channel coefficient matrix and $\mathbf{N}_k$ is AWGN. When no CSI is available at the receiver, the maximum likelihood detector for $\mathbf{G}_k$ based only on the two most recent blocks $\mathbf{Y}_k$ and $\mathbf{Y}_{k-1}$ is

$$\hat{\mathbf{G}}_k = \arg\max_{\mathbf{G}\in\mathcal{G}} \text{ReTr}\left\{\mathbf{G}\mathbf{Y}_k^\dagger\mathbf{Y}_{k-1}\right\}, \tag{4.7}$$

which represents the *standard decoding equation* for DSTM. The fact that $\mathbf{G}_k$ is estimated from the received data without CSI is the key advantage of this encoding strategy.

Numerous papers have been written on the advantages and disadvantages of various group codes for DSTM. The "quality" of a code is generally defined by two

metrics - rate and diversity product. Rate (R) is obviously important as it represents data throughput per given time interval. In contrast, the diversity product directly impacts BER performance of DSTM group codes. The diversity product of a group is a measure of the absolute distance between individual matrices, and is calculated according to

$$\zeta_{\mathcal{G}} = \frac{1}{2} \min_{0 \leq l < l' < L} |\det(\mathbf{G}_l - \mathbf{G}l')|^{\frac{1}{N}}. \tag{4.8}$$

This quantity is bounded by $0 \leq \zeta_{\mathcal{G}} \leq 1$. Any group with $\zeta_{\mathcal{G}} > 0$ is said to have "full diversity", meaning at large SNR no two distinct transmitted blocks, $\mathbf{C}_k$ and $\mathbf{C}_{k+n}$, will have the same received signal, $\mathbf{Y}_k$ and $\mathbf{Y}_{k+n}$. Higher diversity product is therefore associated with reduced BER. The goal in constructing DSTM codes is therefore to find matrix groups $\mathcal{G}$ that offer high rates and high diversity products. DSTM group code design is a rich and well researched topic but will not be discussed in detail in this thesis. The interested reader can find more information in [2] and [4].

4.2 Performance in Aeronautical Telemetry Channels

As discussed in Chapter 3, two key properties of the Alamouti code that make it effective in providing a robust link for aeronautical telemetry are diversity and orthogonality. Diversity in the code allows detection even when the channel between one antenna and the receiver is obstructed. Orthogonality leads to orthogonal transmit radiation patterns during the two time slots, leading to removal of transmission nulls associated with traditional MISO transmission (Figures 3.1 and 3.2). The DSTM codes used in this work offer both high diversity and yield orthogonal transmission matrices, and therefore will offer benefits similar to those observed in conjunction with Alamouti's code.

Figure 4.2 shows the BER performance when using the quaternion code from (4.3) in the telemetry channel. The results from Alamouti's code assuming perfect CSI are also provided for comparison. As expected, DSTM overcomes the antenna self-interference problem much as Alamouti's code does. In fact, at high SNR the differential code outperforms Alamouti's code due to its higher coding advantage [2]. However, it must be remembered that the differential code operates at a lower rate

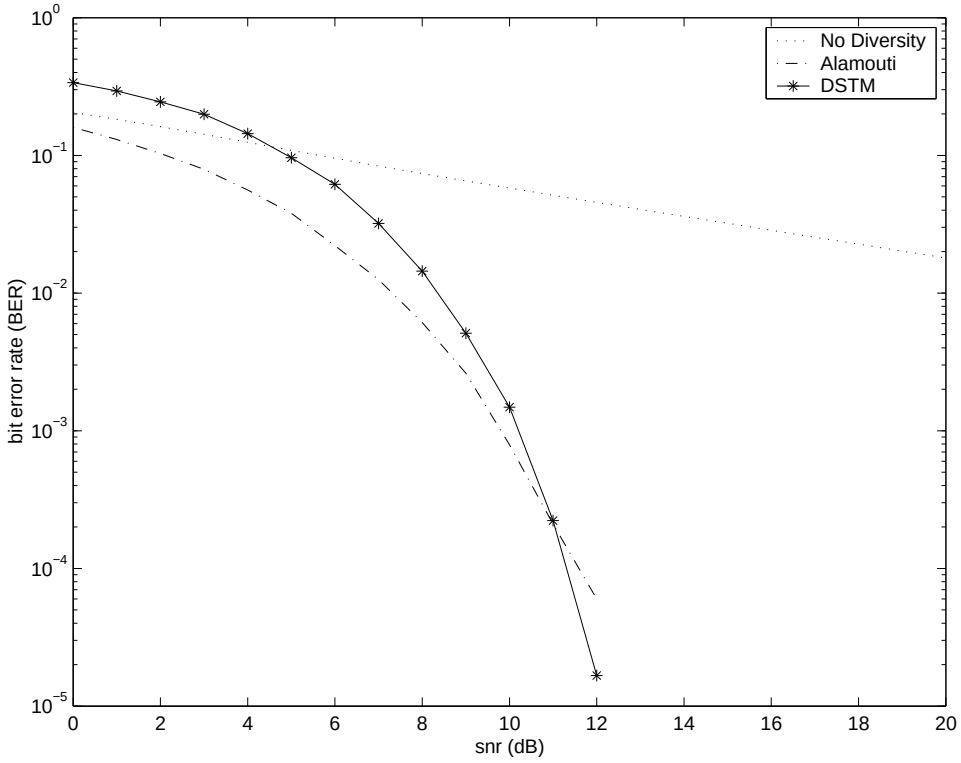

Figure 4.2: Performance curves for several possible transmission schemes.

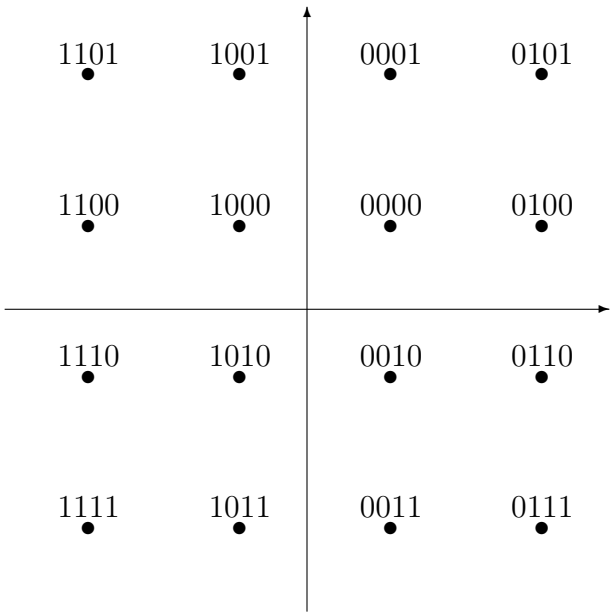

Figure 4.3: Gray encoded 16QAM constellation template.

(1.5) than Alamouti's code (2.0). Therefore, this BER curve does not provide a full indication of the relative performance of these codes.

4.3 DSTM Gray Encoding

For coherent modulation schemes used in SISO transmission, Gray encoding is often used to decrease the number of bit errors per given symbol error. The idea behind Gray encoding is observing that when a symbol is improperly detected, it is most likely to be misdetected as one of the symbols closest to (in a Euclidean sense) the actual transmitted symbol. Therefore, data bits should be mapped to symbols such that there is only one bit different between nearest neighbors in the symbol constellation. This maximizes the probability that there is only one bit error for each symbol error. Figure 4.3 is an example of a Gray encoded constellation template for 16QAM SISO transmission which shows all adjacent symbols differing by a single bit. Further, Figure 4.4 shows the advantage of using Gray encoding with Alamouti's scheme (which uses QPSK symbols) over an arbitrary bit-to-symbol mapping where

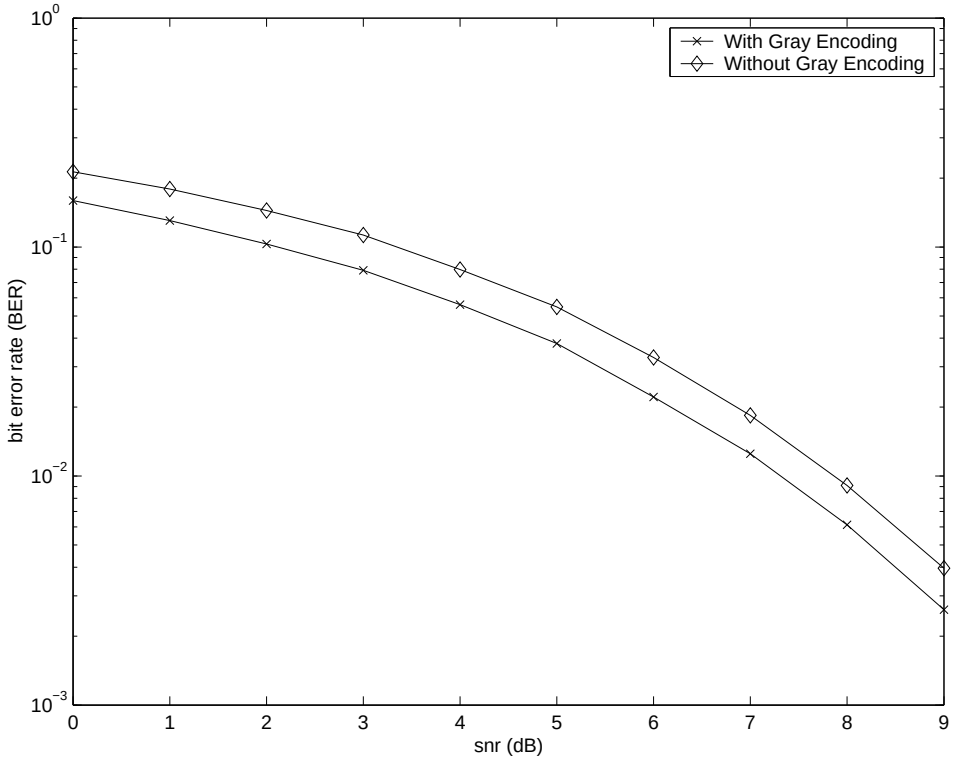

Figure 4.4: Bit error rate for Alamouti's scheme with and without Gray encoding.

neighbors may differ by more than one bit. As can be seen from this plot, Gray encoding provides approximately a 1dB improvement in BER.

This section explores the possibilities of using similar techniques to minimize bit errors per misdetected block when using DSTM.

4.3.1 A Simple Approach

First consider a simple mechanism for implementing Gray encoding to the quaternion code. Intuitively, it seems that a matrix $\mathbf{A}$ will least likely be misdetected as matrix $-\mathbf{A}$ since transmitted symbols in the two matrices are as far apart as possible in the QPSK constellation. Therefore, matrices that are opposites may be encoded so they have *maximal* number of bit differences. This implies that a misdetection will rarely produce the maximum number of bit errors. This works nicely for groups that have N even matrices, $N/2$ of which are opposites of the other $N/2$

Table 4.1: Simple Gray encoding for the rate 1.5 QPSK quaternion group.

Block Code	Data Sequence	Block Code	Data Sequence
$\begin{bmatrix} 1 & 0 \\ 0 & 1 \end{bmatrix}$	000	$\begin{bmatrix} -1 & 0 \\ 0 & -1 \end{bmatrix}$	111
$\begin{bmatrix} j & 0 \\ 0 & -j \end{bmatrix}$	001	$\begin{bmatrix} -j & 0 \\ 0 & j \end{bmatrix}$	110
$\begin{bmatrix} 0 & -1 \\ 1 & 0 \end{bmatrix}$	010	$\begin{bmatrix} 0 & 1 \\ -1 & 0 \end{bmatrix}$	101
$\begin{bmatrix} 0 & j \\ j & 0 \end{bmatrix}$	011	$\begin{bmatrix} 0 & -j \\ -j & 0 \end{bmatrix}$	100

(which is the case for the quaternion group). Encoding can be done in this situation since the binary numbers $\{0, \ldots, N-1\}$ have $N/2$ pairs of numbers that are binary complements. The quaternion group can be encoded as show in Table 4.1.

Figure 4.5 shows the BER performance of this encoding scheme relative to a random bit-to-matrix mapping. These results show that this simple encoding scheme is only mildly successful as it does not achieve the same performance enhancement as observed in Figure 4.4. This is due to the fact that only non-adjacent matrices were addressed for encoding rather than adjacent matrices.

4.3.2 Monte Carlo Approach

Not only does the simple mapping proposed above fall short of the gains expected from Gray encoding, but also in some cases it is unusable since not all codes have N/2 pairs of matrices that are opposites. Therefore, a more sophisticated approach is needed in order for Gray encoding to provide maximum benefits when

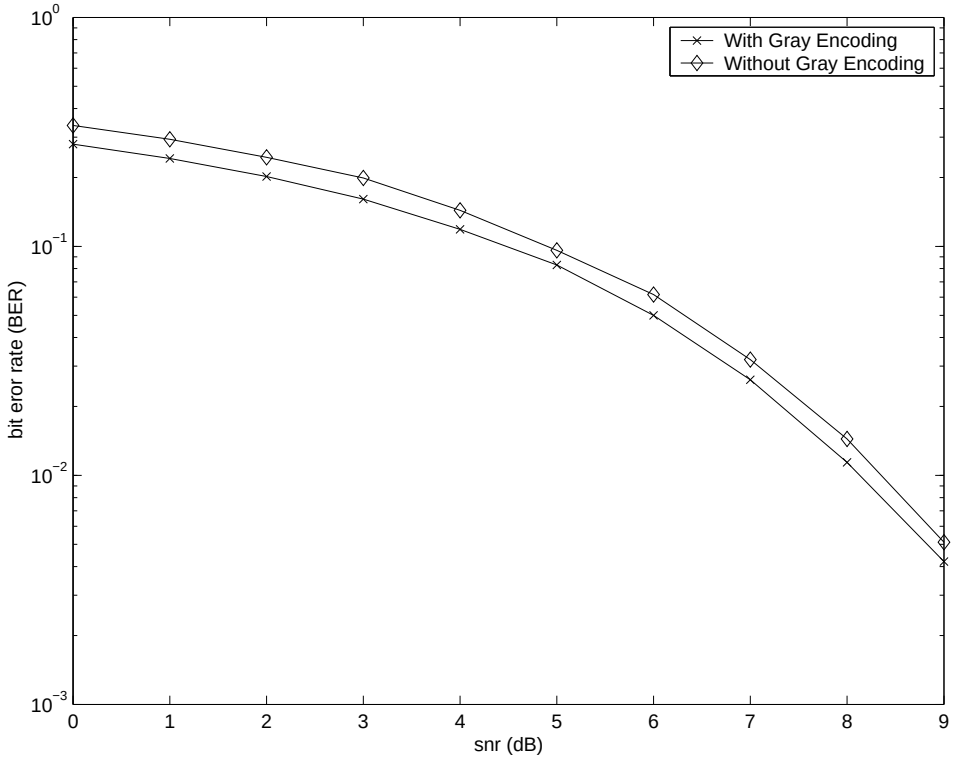

Figure 4.5: Bit error rate for the quaternion code using simple Gray encoding.

Table 4.2: Tabular results for the rate 2.0 quaternion code.

Matrix	G_0	G_1	G_2	G_3	G_4	G_5	G_6	G_7	G_8	G_9	G_{10}	G_{11}	G_{12}	G_{13}	G_{14}	G_{15}
G_0	1549	71	80	36	425	456	81	64	1	69	73	45	9	9	70	67
G_1	76	1592	46	76	55	75	7	440	66	1	44	65	76	68	438	3
G_2	73	45	1533	77	74	80	9	10	77	32	3	70	49	64	429	404
G_3	44	65	84	1563	419	7	58	83	45	80	70	6	5	436	64	68
G_4	447	87	73	415	1560	43	83	75	7	62	74	9	5	39	75	76
G_5	452	72	66	7	37	1630	68	72	6	84	63	439	35	2	71	74
G_6	69	9	12	63	75	69	1637	37	68	402	408	77	69	87	4	40
G_7	76	422	6	72	71	61	39	1626	67	6	473	76	75	88	33	2
G_8	7	62	74	35	5	9	64	72	1599	65	77	34	452	443	77	66
G_9	66	3	36	63	71	67	405	7	71	1672	42	75	79	97	4	416
G_{10}	72	44	5	81	76	63	374	415	73	56	1612	55	53	83	7	6
G_{11}	50	70	64	1	5	472	79	76	40	62	70	1572	418	17	76	71
G_{12}	10	83	76	5	5	36	72	68	434	61	55	418	1603	31	62	72
G_{13}	11	62	74	441	44	1	67	77	426	79	74	9	40	1581	84	76
G_{14}	72	407	397	68	74	93	5	41	77	10	3	61	75	68	1596	38
G_{15}	72	15	443	53	53	67	49	2	72	427	6	73	75	58	40	1654
Totals	3146	3109	3069	3056	3049	3229	3097	3165	3129	3168	3147	3084	3118	3171	3130	3133

applied to DSTM. We therefore propose an approach that uses a Monte Carlo simulation to tabulate the frequency with which each matrix is detected when a specific matrix has been sent. For this simulation data were mapped to the 16 element, rate $R = 2.0$, DSTM quaternion code and transmitted through the complex Gaussian fading channel , as discussed in Appendix A. This was done at an SNR of 5 dB in order to produce a wider spread in misdetections and hence better statistics.

Table 4.2 shows the tabulated results of the Monte Carlo simulation where the matrix subscript denotes the bit mapping (i.e. $\mathbf{G}_0 -> 0000, \mathbf{G}_1 -> 0001$ etc.).. The seventh column ($\mathbf{G}_6$) will be used as an example in order to understand Table 4.2. Of the $5 * 10^4$ symbols ($2 * 10^5$ bits) that were sent 3097 of them were the matrix $\mathbf{G}_6$ (the bit sequence 0110). Column 7 shows that of the 3097 times that $\mathbf{G}_6$ was sent it was detected correctly 1637 times and misinterpreted as matrix $\mathbf{G}_0$ 81 times, as matrix $\mathbf{G}_1$ seven times, and so on. From column 7 it is also shown that matrix $\mathbf{G}_6$ was most often misdetected as two other matrices: $\mathbf{G}_9$ and $\mathbf{G}_{10}$. Eight other matrices share a substantially high misdetection rate: $\mathbf{G}_1$, $\mathbf{G}_3$, $\mathbf{G}_4$, $\mathbf{G}_5$, $\mathbf{G}_8$, $\mathbf{G}_{11}$, $\mathbf{G}_{12}$ and $\mathbf{G}_{13}$. The remaining matrices $\mathbf{G}_1$, $\mathbf{G}_2$, $\mathbf{G}_7$, $\mathbf{G}_{14}$, and $\mathbf{G}_{15}$ have a lower number of misdetections. Surprisingly, $\mathbf{G}_9$ and $\mathbf{G}_{10}$ comprise over one-half of all misdetections (779 out of 1460, or 53%) while the other 13 matrices produce the other half of matrix errors. Further inspection of Table 4.2 reveals that the single matrix $\mathbf{G}_9$ (or the bit sequence 1001) was the most misdetected matrix for matrix $\mathbf{G}_6$ (or the bit sequence 0110). This

results, unnecessarily, in *four bit errors per misdetection* when $\mathbf{G}_9$ was decided over $\mathbf{G}_6$. A more detailed perusal of Table 4.2 shows that each matrix in $\mathcal{G}$ has two distinct matrices that can be termed "adjacent", 11 of which are close neighbors and two of which are furthest out.

Using these simulation results, DSTM matrices can be defined as "adjacent", much like SISO symbols are adjacent, and therefore can be Gray encoded. Ideally, in a group with N matrices each matrix would have $\log_2(N)$ unique adjacent matrices. Were this the case then a Gray encoded QAM constellation could be used as a template for adjacent matrices and Gray encoded (see Figure 4.3).

For this example the obvious choice would be to use the Gray encoded 16QAM constellation template since there are 16 matrices in this code. The Monte Carlo simulation results, however, do not produce the ideal four adjacent matrices per matrix. Having only two adjacent matrices does give some advantage in that we have room to choose from quasi-adjacent neighbors in order to make them fit onto the Gray encoded mapping. Table 4.3 shows each matrix and their four chosen adjacent matrices such that the 16QAM Gray encoded constellation template can be used.

By comparing Figures 4.3 and 4.6 and cross-referencing them with Table 4.3 it can be seen that the quaternion code maps perfectly and completely onto the 16QAM Gray encoded constellation. This provides only one bit difference between all adjacent matrices and the two matrices with the furthest distance are never adjacently mapped. Figure 4.7 shows the BER improvement using Gray encoding with the rate 2.0 quaternion group code. This figure shows that a 1dB gain advantage is possible with DSTM, which is similar to the result obtained when applying Gray encoding to Alamouti's code.

4.3.3 Analytical Approach

An analytical approach to DSTM Gray encoding may also be possible for some group codes. When calculating the diversity product with Eq. (4.8) each matrix will share a certain distance with all other matrices in a group. Ideally, two matrices with a low product distance would be considered adjacent and would have a direct correlation

Table 4.3: Adjacent matrices for the rate 2.0 quaternion code.

Matrix	Adjacent Matrices
G_0	G_4, G_5, G_{10}, G_1
G_1	G_0, G_{11}, G_{14}, G_7
G_2	G_{14}, G_{15}, G_7, G_3
G_3	G_4, G_2, G_{10}, G_{13}
G_4	G_0, G_{14}, G_3, G_8
G_5	G_6, G_0, G_4, G_{11}
G_6	G_{13}, G_{10}, G_5, G_9
G_7	G_2, G_9, G_1, G_{10}
G_8	G_5, G_4, G_{13}, G_{12}
G_9	G_{15}, G_6, G_{11}, G_7
G_{10}	G_3, G_7, G_0, G_6
G_{11}	G_9, G_5, G_{12}, G_1
G_{12}	G_{11}, G_8, G_{15}, G_{14}
G_{13}	G_8, G_3, G_6, G_{15}
G_{14}	G_1, G_{12}, G_2, G_4
G_{15}	G_{12}, G_{13}, G_9, G_2

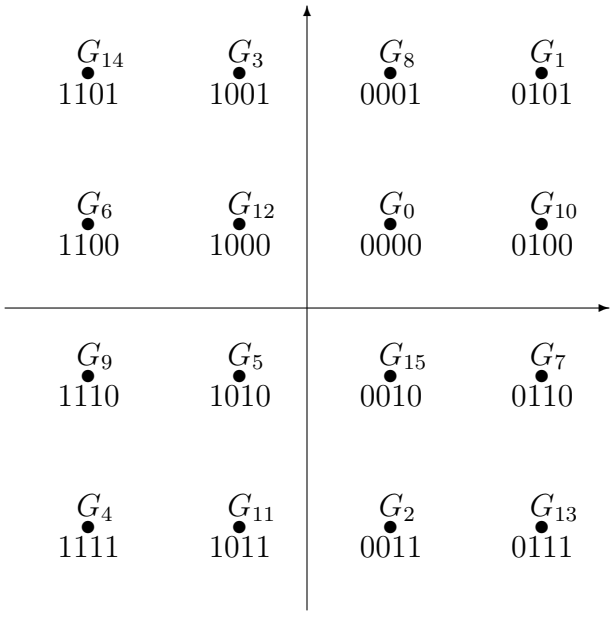

Figure 4.6: The rate 2.0 quaternion code mapped to a Gray encoded 16QAM constellation.

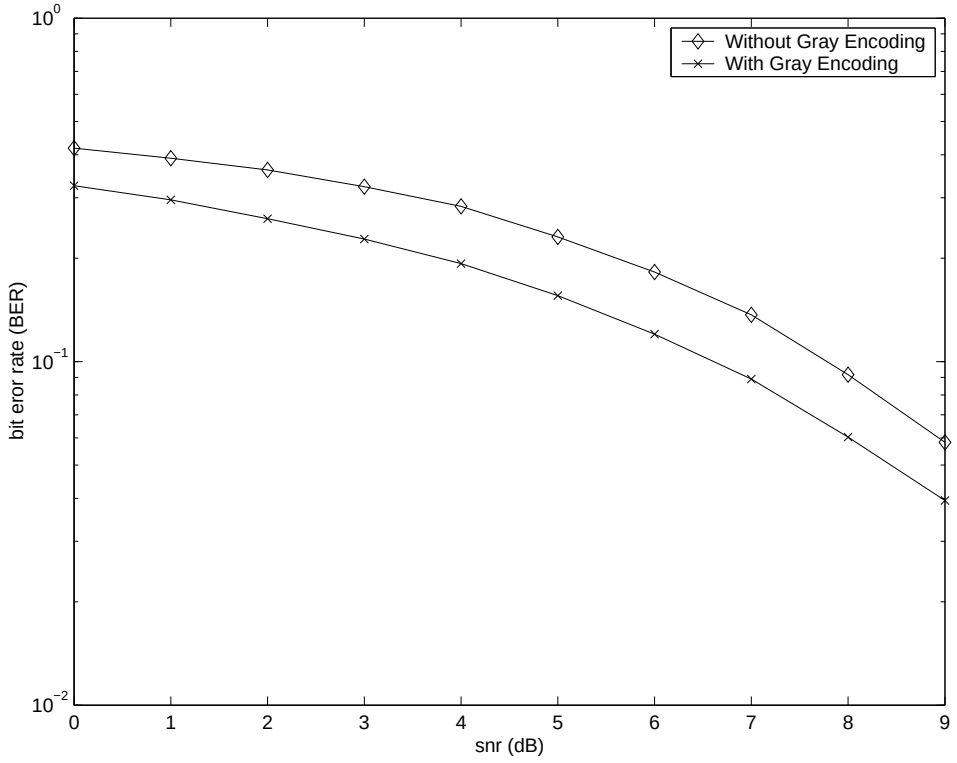

Figure 4.7: Bit error rate for the rate 2.0 quaternion code with and without Gray encoding.

Table 4.4: Matrix by matrix product distance for the rate 2.0 quaternion code.

Matrix	G_0	G_1	G_2	G_3	G_4	G_5	G_6	G_7	G_8	G_9	G_{10}	G_{11}	G_{12}	G_{13}	G_{14}	G_{15}
G_0	0	0.71	0.71	0.71	0.38	0.38	0.71	0.71	1.00	0.71	0.71	0.71	0.92	0.92	0.71	0.71
G_1	0.71	0	0.71	0.71	0.71	0.71	0.92	0.38	0.71	1.00	0.71	0.71	0.71	0.71	0.38	0.92
G_2	0.71	0.71	0	0.71	0.71	0.71	0.92	0.92	0.71	0.71	1.00	0.71	0.71	0.71	0.38	0.38
G_3	0.71	0.71	0.71	0	0.38	0.92	0.71	0.71	0.71	0.71	0.71	1.00	0.92	0.38	0.71	0.71
G_4	0.38	0.71	0.71	0.38	0	0.71	0.71	0.71	0.92	0.71	0.71	0.92	1.00	0.71	0.71	0.71
G_5	0.38	0.71	0.71	0.92	0.71	0	0.71	0.71	0.92	0.71	0.71	0.38	0.71	1.00	0.71	0.71
G_6	0.71	0.92	0.92	0.71	0.71	0.71	0	0.71	0.71	0.38	0.38	0.71	0.71	0.71	1.00	0.71
G_7	0.71	0.38	0.92	0.71	0.71	0.71	0.71	0	0.71	0.92	0.38	0.71	0.71	0.71	0.71	1.00
G_8	1.00	0.71	0.71	0.71	0.92	0.92	0.71	0.71	0	0.71	0.71	0.71	0.38	0.38	0.71	0.71
G_9	0.71	1.00	0.71	0.71	0.71	0.71	0.38	0.92	0.71	0	0.71	0.71	0.71	0.71	0.92	0.38
G_{10}	0.71	0.71	1.00	0.71	0.71	0.71	0.38	0.38	0.71	0.71	0	0.71	0.71	0.71	0.92	0.92
G_{11}	0.71	0.71	0.71	1.00	0.92	0.38	0.71	0.71	0.71	0.71	0.71	0	0.38	0.92	0.71	0.71
G_{12}	0.92	0.71	0.71	0.92	1.00	0.71	0.71	0.71	0.38	0.71	0.71	0.38	0	0.71	0.71	0.71
G_{13}	0.92	0.71	0.71	0.38	0.71	1.00	0.71	0.71	0.38	0.71	0.71	0.92	0.71	0	0.71	0.71
G_{14}	0.71	0.38	0.38	0.71	0.71	0.71	1.00	0.71	0.71	0.92	0.92	0.71	0.71	0.71	0	0.71
G_{15}	0.71	0.92	0.38	0.71	0.71	0.71	0.71	1.00	0.71	0.38	0.92	0.71	0.71	0.71	0.71	0

with probability of misdetection. Using this definition of adjacent, the matrices may be mapped to the Gray encoded constellation as was done in the previous section.

Table 4.4 shows the matrix product distance for all possible combinations in the rate 2.0 quaternion group. Notice the zeros down the diagonal since the product distance of a matrix with itself is always zero. Close comparison of Table 4.2 with Table 4.4 shows exactly the match that was expected. The seventh column will again be used as an example. Matrices $\mathbf{G}_9$ and $\mathbf{G}_{10}$ both have the smallest product distance from matrix $\mathbf{G}_6$, and matrices $\mathbf{G}_1$, $\mathbf{G}_2$, and $\mathbf{G}_{13}$ have the highest product distance. Comparing column 7 from Table 4.4 and column 7 from Table 4.2 does in fact show a direct correlation between product distances and frequency of misdetections as expected. Further column by column comparisons between the two tables will show the same results for each matrix. Therefore, this analysis confirms the mapping created using the Monte Carlo simulation and provides a faster method for mapping adjacent matrices.

For any N element DSTM quaternion group $\mathcal{G}$ it has been shown that adjacent matrices can be defined as those with the lowest product distances. After defining adjacent matrices, each matrix can be Gray encoded by using the appropriate QAM constellation as a template. This ensures that the most often misdetected matrices will produce at most one bit error. It should also be mentioned that DSTM Gray encoding is not confined to QAM constellation templates. Where QAM symbols are

confined to a 2-dimensional space DSTM block matrices are not. For example, an eight element DSTM group where each matrix has three adjacencies can still be Gray encoded though the 8PSK template would only allow for two adjacencies.

4.4 Alamouti Versus DSTM

Alamouti's space-time code and differential space-time modulation are orthogonal transmit diversity schemes which have been shown to overcome the self-interference problem detailed in this thesis. Difficulty now arises in comparing these two different coding schemes as there are numerous metrics in deciding which scheme can be classified as "better". At the risk of neglecting other important factors the following criteria for a "better" scheme will be considered:

1. Bit error performance
2. Data throughput
3. Facility of hardware implementation

Bit error performance has already been well formulated in previous chapters but will be reiterated here for completeness. Figure 4.2 shows the BER curves for the three transmission schemes evaluated. Both Alamouti's scheme and DSTM perform exceptionally well in the telemetry channel, with DSTM offering a higher coding advantage and therefore a lower BER at higher SNR.

In order to accurately model data throughput, the bits used to acquire channel information at the receiver (training bits which contain no data information) will not be included in total transmission throughput. In other words, the total number of correctly detected bits will not include training data. For this comparison 10^5 symbols were randomly generated and transmitted through the telemetry channel using both Alamouti and DSTM for various data transmission rates. For Alamouti's code, four training symbols were sent per training interval. Figure 4.8 shows throughput in terms of percent of correctly decoded bits versus training frequency. Observe that DSTM curves appear as horizontal lines since they do not require channel estimates and therefore are independent of training intervals.

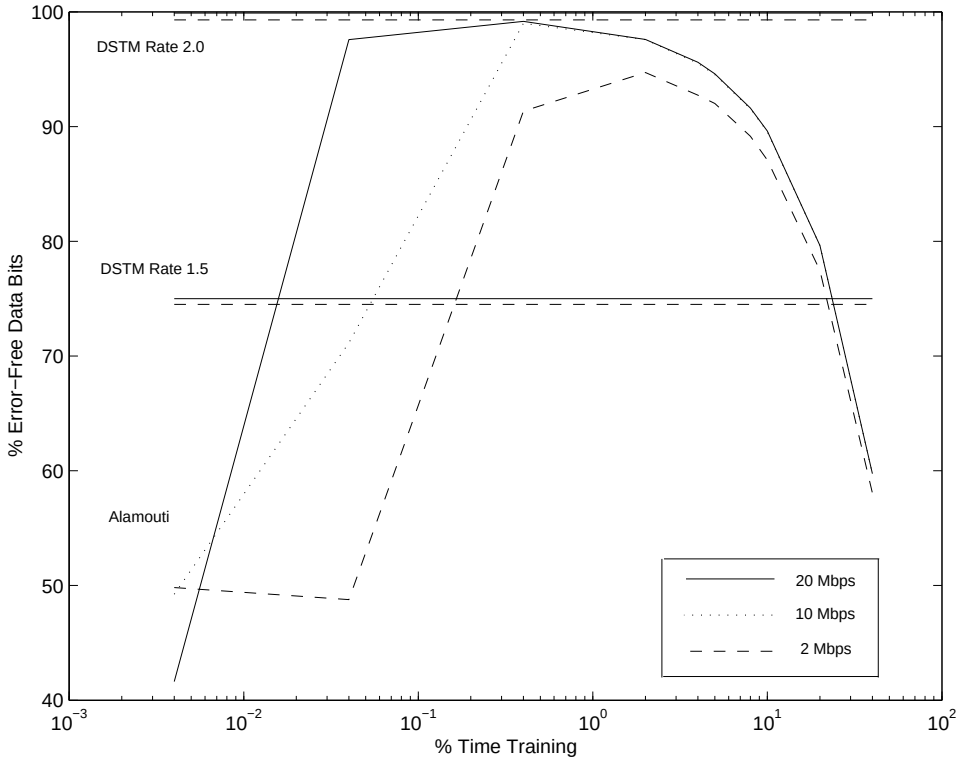

Figure 4.8: Throughput comparison between DSTM and Alamouti codes.

An initial inspection of Figure 4.8 reveals that both codes perform as expected by evaluations done in previous chapters with several additional interesting comparisons. First, observe that changing the data rate from 2 Mbs to 20 Mbs results in an effective decrease in change of the channel coefficients between symbol periods. DSTM is inherently impervious to changes in the channel as can be seen by the fact that the fractional throughput has minimal change between 20 Mbs and 2 Mbs transmit rates. Alamouti, on the other hand, is significantly affected by the channel as is demonstrated by the fact that more training is required for lower data rates to achieve maximum throughput. Another interesting observation is that all Alamouti curves converge to the same line. When channel estimates are good enough (i.e. when enough training has been done to predict the channel sufficiently) Alamouti's scheme produces almost no errors and the drop-off in throughput is strictly due to data loss from training symbols.

The third comparison metric is the ease with which these modulators and detectors can be built. On the transmission side both schemes can ideally be created with simple lookup tables and appropriate symbol mappings. The complexity occurs, for both schemes, at the receiver. A DSTM receiver is relatively simple as it only requires the last two received blocks, a multiplier, and a lookup table. The eight matrix multiplies required at the detector from Eq. (4.7) can be simplified by observing that maximization of the trace using each matrix in the quaternion group is just maximizing the sum of the real and/or imaginary parts of the diagonal or off-diagonal elements. An Alamouti receiver requires a single matrix multiply, but it must also accommodate the training symbols and perform channel coefficient estimation. Furthermore, the scheme must determine a suitable training interval which can vary with the maneuvering of the air vehicle. This training requirement will also add some complexity at the transmitter.

Difficulty now arises when trying to decide the "best" coding scheme to use. BER performance is so similar that it does not motivate the choice of one code over the other. If we only define best throughput as the optimizing criteria than Alamouti's scheme would probably be considered best. At the optimal training frequency

Alamouti's scheme transmits at an almost 50% higher rate than DSTM when using the same modulation symbols. And, when training between .1% and 25% at 2Mbs, Alamouti's code still achieves a higher total throughput. Rate 2.0 DSTM appears to be better overall but may not be suitable for all applications as is uses symbols in the 8PSK constellation. A throughput comparison between Alamouti and the rate 2.0 quaternion group is not informative since an 8PSK Alamouti code would be rate 3.0. If a DSTM group could be found that had a basis in the QPSK constellation as well as rate 2.0 then DSTM would likely be "better" on all accounts.

Chapter 5

Space-Time Codes with Offset Modulation

The United States Department of Defense sponsors the Advanced Range Telemetry (ARTM) program for advances and testing in military aeronautic technologies. Included in the scope of ARTM is the improvement of wireless telemetry links between test flight vehicles and data gathering ground stations. ARTM promotes military standards (MIL-STD) for government test bases that use such wireless links.

Shaped offset quadrature phase shift keying (SOQPSK) is often employed in ARTM wireless systems as it increases spectral efficiency and provides a nearly constant envelope characteristic which is desirable since the transmitter amplifier can operate outside its linear range. However, the offset nature of the modulation creates difficulty for the space-time coding strategies considered in this thesis. Since SOQPSK will have an increasing presence in Air Force systems, it is important that the space-time codes be applicable to this modulation.

This chapter will provide a system level overview of the ARTM SOQPSK modulation scheme and how this modulation impacts the implementation of the space-time codes. The possibility of integrating Alamouti's scheme and DSTM on both the transmit and receive ends of an SOQPSK system will be explored.

5.1 SOQPSK Transmission

Figure 5.1 shows a simplified block diagram of the ARTM SOQPSK transmit system currently being used on test flight aircraft. We first emphasize again that both transmit antennas emit the same waveforms discussed in Chapter 2. The first system block accepts information bits as input and maps them to symbols by way of

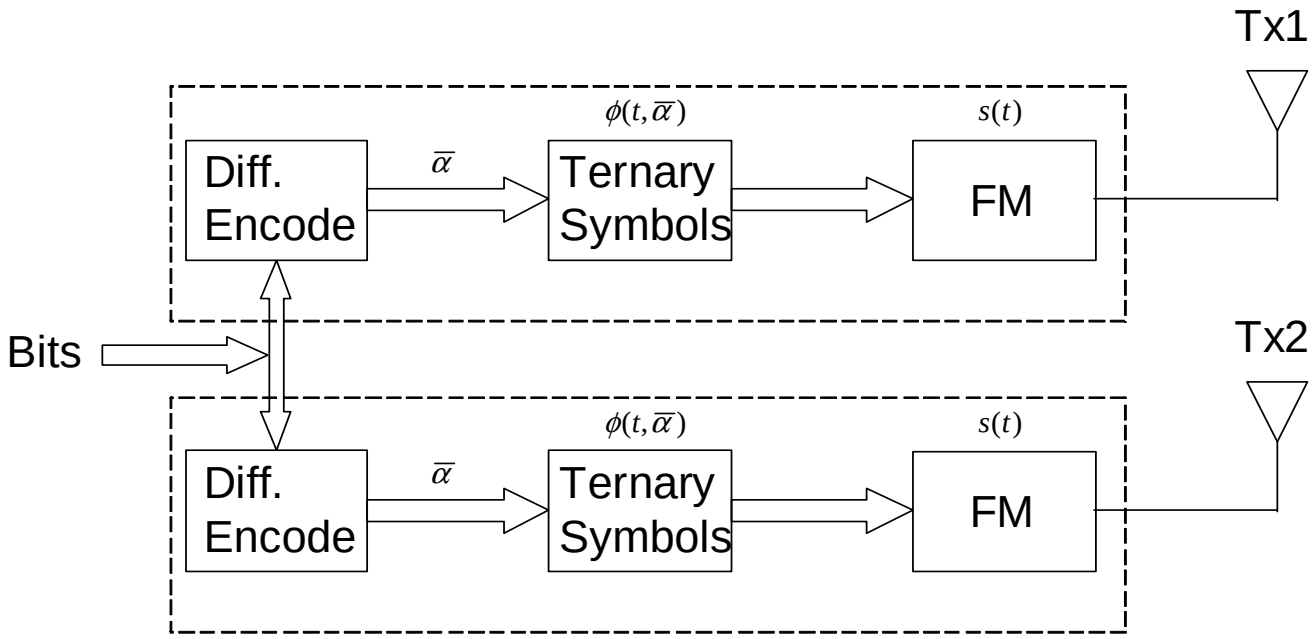

Figure 5.1: Modulation branches of an ARTM SOQPSK transmitter.

the differential bit encoding equations

$$\begin{aligned} I_{2n} &= -b_{2n} \oplus Q_{2n-1} \\ Q_{2n+1} &= b_{2n+1} \oplus I_{2n}, \end{aligned} \tag{5.1}$$

where n is the integer symbol time, b are data bits with values ± 1, and I and Q, also with values ± 1, are the inphase and quadrature components of the symbols in the modulation constellation. The exclusive or operator $\oplus$ is defined by

$$A \oplus B = \begin{cases} 1 & A = B \\ -1 & A \neq B. \end{cases} \tag{5.2}$$

This bit encoder introduces memory into the system, demonstrated by the dependence of future symbols on previous ones. This has been shown to improve overall spectral efficiency of the system as well as introduce a natural half-symbol time offset between the inphase and quadrature channels.

The i^{th} differentially encoded QPSK symbol transition can be equivalently represented as a ternary symbol with possible values, $\alpha_i = -1, 0, 1$, with the value of

α_i indicating that the phase should change by $\pi/2$, 0, or $-\pi/2$ radians respectively. It should be noted that the ternary symbol time index, i, is bit time and not symbol time. Data mapped ternary symbols are shown by the vector $\bar{\alpha}$ in the SOQPSK system block diagram. After these mappings a phase waveform is created with

$$\phi(t, \bar{\alpha}) = \frac{\pi}{2} \int_{-\infty}^{t} \sum_{i=-\infty}^{i=\infty} \alpha_i g(\tau - iT/2) d\tau. \tag{5.3}$$

where $g(t)$ is the frequency pulse shape and T is the symbol time. The signal is then frequency modulated by

$$s(t) \sim \cos\left(2\pi f_0 t + \phi(t, \bar{\alpha})\right), \tag{5.4}$$

at the carrier frequency f_0, and transmitted simultaneously from both antennas.

The following sections outline the difficulties in integrating space-time codes with the SOQPSK modulator and propose potential space-time code implementation strategies suitable for this modulation scheme.

5.2 Differential Bit Encoding

The first issue can be observed by examining in more detail the memory involved in differential bit encoding from Eq. (5.1). Recall that Alamouti's scheme (see Table 3.1) and DSTM (see Figure 4.1) specify the symbols in the second transmission slot of the code block based on the symbols in the first transmission slot. However, the differential bit encoding imposes its own constraint on these symbols, therefore requiring modification of the space-time encoding scheme for implementation with this modulation.

In order to use space-time codes with SOQPSK modulation we need the freedom of producing the desired symbols at each symbol time on the output and not be constrained by previous data bits. This should in general be possible, since the offset transition allows movement from a point in the constellation to any other point over a symbol time (2 bit times = 2 phase transitions). Our goal is then to find a precoding strategy for the data bits such that the space-time codes and differential bit encoding are compatible.

Table 5.1: Alamouti's encoding scheme for two transmit antennas over three symbol periods.

symbol time	antenna 1	antenna 2
n - 1	$-s_{n-1}^*$	s_{n-2}^*
n	s_n	s_{n+1}
n + 1	$-s_{n+1}^*$	s_n^*

For Alamouti's scheme, consider output symbols from the differential encoding block (Eq. (5.1)) rewritten, without loss of generality, as

$$s_n^{(p)} = I_{2n}^{(p)} + jQ_{2n+1}^{(p)} = -b_{2n}^{(p)} \oplus Q_{2n-1}^{(p)} + j(b_{2n+1}^{(p)} \oplus I_{2n}^{(p)}) \tag{5.5}$$

where $s_n^{(p)}$ represents a QPSK symbol on channel p at symbol time n with I and Q components offset by half a symbol period and $b_{2n}^{(p)}$ are data bits. Equation (5.1) naturally introduces a time offset unlike equation (5.5) which assumes the quadrature symbols will be offset after symbol creation.

Since we are dealing with memory in differential bit encoding, Alamouti's scheme needs to be addressed not only with the current and future time steps but also the previous transmission time as shown in Table 5.1. Using Eq. (5.5) and Table 5.1 the desired symbols $s_n^{(p)}$ over an Alamouti period given differential bit encoding can be written as

$$\begin{aligned}
s_n^{(1)} &= s_n &&= -b_{2n}^{(1)} \oplus Q_{2n-1}^{(1)} + j(b_{2n+1}^{(1)} \oplus I_{2n}^{(1)}) \\
s_n^{(2)} &= s_{n+1} &&= -b_{2n+2}^{(2)} \oplus Q_{2n+1}^{(2)} + j(b_{2n+3}^{(2)} \oplus I_{2n+2}^{(2)}) \\
s_{n+1}^{(1)} &= -s_{n+1}^* &&= b_{2n+2}^{(1)} \oplus Q_{2n+1}^{(2)} + j(b_{2n+3}^{(1)} \oplus I_{2n+2}^{(2)}) \\
s_{n+1}^{(2)} &= s_n^* &&= -b_{2n}^{(2)} \oplus Q_{2n-1}^{(1)} - j(b_{2n+1}^{(2)} \oplus I_{2n}^{(1)})
\end{aligned}$$

where s_n with no superscript refers to Alamouti mapped symbols in the original datastream.

Consider the following derivation for finding the $b_{2n}^{(1)}$ bits (i.e. the bits at time $2n$ that will be sent through the differential encoder on channel 1 in order to produce Alamouti symbols on the output of the transmitter). Using Eq. (5.6) and looking

initially at the first symbol

$$s_n^{(1)} = s_n \quad = \quad -b_{2n}^{(1)} \oplus Q_{2n-1}^{(1)} + j(b_{2n+1}^{(1)} \oplus I_{2n}^{(1)}) \tag{5.6}$$

and more specifically at the inphase component

$$I_{2n}^{(1)} = -b_{2n}^{(1)} \oplus Q_{2n-1}^{(1)} \tag{5.7}$$

and realizing that $I_{2n}^{(1)}$ (the real part of s_n) and $Q_{2n-1}^{(1)}$ (the imaginary part of s_{n-1}^*) are known we can solve for $b_{2n}^{(1)}$ with

$$b_{2n}^{(1)} = -I_{2n}^{(1)} \oplus Q_{2n-1}^{(1)}. \tag{5.8}$$

Similar treatments can be done for the other bits on both channels producing the following update equations

$$\begin{aligned}
b_{2n}^{(1)} &= -I_{2n}^{(1)} \oplus Q_{2n-1}^{(1)} \\
b_{2n+1}^{(1)} &= I_{2n}^{(1)} \oplus Q_{2n+1}^{(1)} \\
b_{2n+2}^{(1)} &= I_{2n+2}^{(2)} \oplus Q_{2n+1}^{(1)} \\
b_{2n+3}^{(1)} &= -I_{2n+2}^{(2)} \oplus Q_{2n+3}^{(2)} \\
b_{2n}^{(2)} &= I_{2n}^{(2)} \oplus Q_{2n-1}^{(2)} \\
b_{2n+1}^{(2)} &= I_{2n}^{(2)} \oplus Q_{2n+1}^{(2)} \\
b_{2n+2}^{(2)} &= -I_{2n+2}^{(1)} \oplus Q_{2n+1}^{(2)} \\
b_{2n+3}^{(2)} &= -I_{2n+2}^{(1)} \oplus Q_{2n+3}^{(1)}.
\end{aligned} \tag{5.9}$$

It is then a simple matter of introducing one more block to our system which precodes the data bits according to the update equations as shown in Figure 5.2. Notice that the output symbols on each channel are now different and will correspond to an Alamouti encoded system.

5.3 Offset Modulation

The second issue that arises when dealing with SOQPSK waveforms can be seen by examining the sampled filter outputs at the receiver of a standard non-shaped

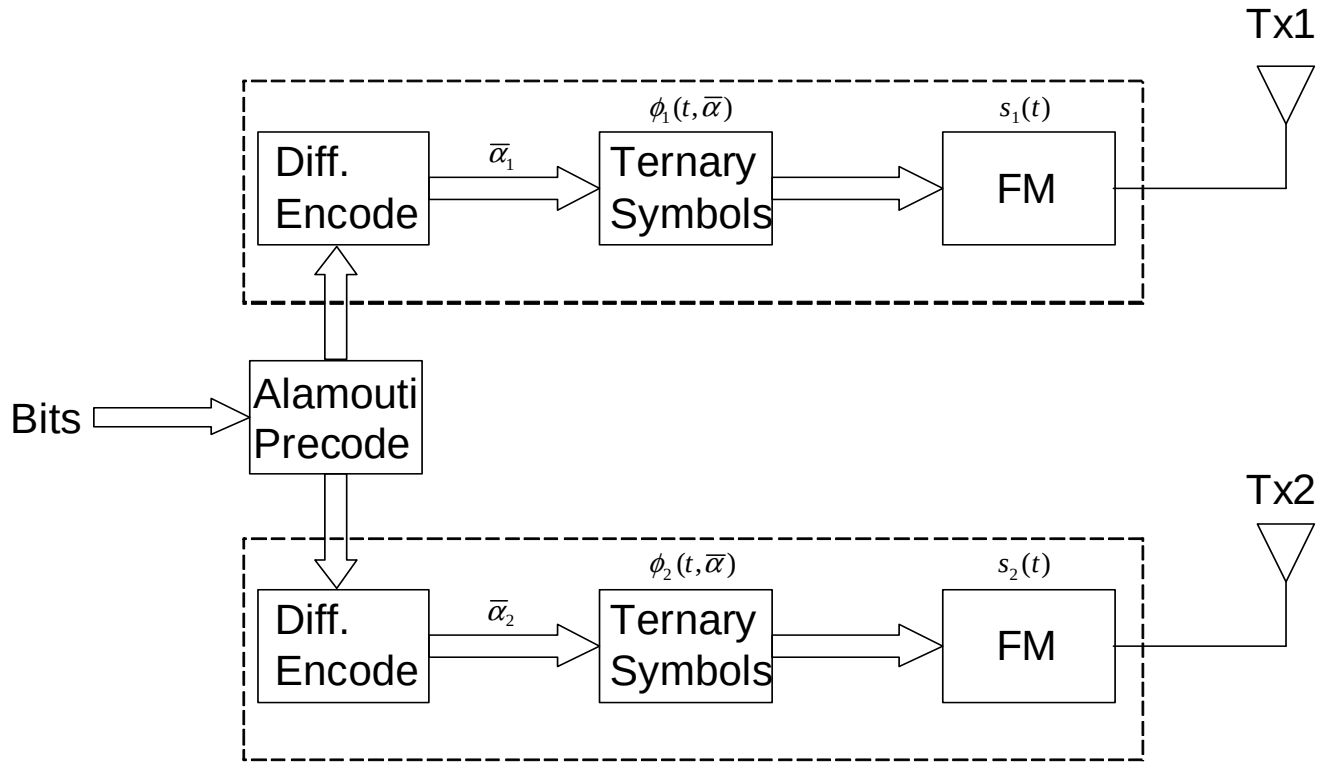

Figure 5.2: Modulation branches of an ARTM SOQPSK transmitter with Alamouti pre-coder.

OQPSK system. In [5] it is shown that when Alamouti's encoding is used at the transmitter the sampled filter outputs, $\mathbf{x} = \{x(n), x(n+\frac{1}{2}), x(n+1), x(n+\frac{3}{2})\}$, at the receiver will be

$$\mathbf{x} = \begin{bmatrix} h_1[a_n + jR_p(\frac{T_s}{2})b_{n-1} + R_p(\frac{-T_s}{2})b_n] + h_2[a_{n+1} + jR_p(\frac{T_s}{2})b_{n-2} + jR_p(\frac{-T_s}{2})b_{n+1}] \\ h_1[jb_n + R_p(\frac{T_s}{2})a_n - R_p(\frac{-T_s}{2})a_{n+1}] + h_2[jb_{n+1} + R_p(\frac{T_s}{2})a_{n+1} - R_p(\frac{-T_s}{2})a_n] \\ h_1[-a_{n+1} + jR_p(\frac{T_s}{2})b_n + R_p(\frac{-T_s}{2})b_{n+1}] + h_2[ja_n + R_p(\frac{T_s}{2})b_{n+1} - R_p(\frac{-T_s}{2})b_n] \\ h_1[jb_{n+1} - jR_p(\frac{T_s}{2})a_{n+1} + R_p(\frac{-T_s}{2})a_{n+2}] + h_2[-jb_n + R_p(\frac{T_s}{2})a_n + R_p(\frac{-T_s}{2})a_{n+3}] \end{bmatrix} \tag{5.10}$$

where h_1 and h_2 are the channel coefficients $R_p(\tau)$ is the matched filter pulse shape response and a_n and b_n are the real and imaginary components of the QPSK symbol s_n at symbol time n. Compare this to the matched filter outputs, $\mathbf{x} = \{x(n), x(n+1)\}$, of the non-offset QPSK Alamouti receiver

$$\mathbf{x} = \begin{bmatrix} h_1[a_n + jb_n] + h_2[a_{n+1} + jb_{n+1}] \\ h_1[a_{n+1} - jb_{n+1}] + h_2[a_n - jb_n] \end{bmatrix} = \begin{bmatrix} h_1 & h_2 \\ h_1^* & -h_2^* \end{bmatrix} \begin{bmatrix} s_n \\ s_{n+1} \end{bmatrix}. \tag{5.11}$$

As can be seen from Eqs. (5.10) and (5.11) the filter outputs for OQPSK are dependent on previous, current, and future symbols while outputs from QPSK modulation are only dependent on the current symbols of an Alamouti period. Also, Eq. (5.11) shows the orthogonality of Alamouti's code which is missing from the OQPSK outputs. These problems make use of the standard Alamouti detector, Eqs. (3.6) and (3.7), impossible for an offset modulation scheme.

5.4 SOQPSK Alamouti Detection

We need to develop a new detection approach for Alamouti signaling with SOQPSK modulation. This section suggests two such methods and demonstrates their respective performances.

5.4.1 A Simple Detector

Consider two symbols, denoted s_n and s_{n+1}, encoded with Alamouti's strategy and transmitted from two SOQPSK transmitters. Eq. (5.10) showed matched filter

outputs for OQPSK modulation which can be written more generally as

$$\begin{aligned} x(n) &= h_1[w_0(s_{n-N_0},\ldots,s_{n+N_0})] + h_2[w_1(s_{n-N_2},\ldots,s_{n+N_2})] && (5.12)\\ x([n+\frac{1}{2}]) &= h_1[w_2(s_{n-N_2},\ldots,s_{n+N_2})] + h_2[w_3(s_{n-N_4},\ldots,s_{n+N_4})] && (5.13)\\ x([n+1]) &= h_1[w_4(s_{n-N_4},\ldots,s_{n+N_4})] + h_2[w_5(s_{n-N_6},\ldots,s_{n+N_6})] && (5.14)\\ x([n+\frac{3}{2}]) &= h_1[w_6(s_{n-N_6},\ldots,s_{n+N_6})] + h_2[w_7(s_{n-N_8},\ldots,s_{n+N_8})] && (5.15) \end{aligned}$$

where $w_i(\cdot)$ are weighting functions dependent on up to N_i past and future symbols. This non-causality occurs since the SOQPSK pulse shape does not satisfy the no intersymbol interference (ISI) criterion and causes symbol overlap between filter samples. There are eight different weighting functions since the $2N_i$ temporally adjacent symbols for each sampled output are different.

It can be shown that equations (5.12) and (5.15) are in fact corrupted by previous and/or future symbols but equations (5.13) and (5.14) *are essentially only dependent on the symbols within the Alamouti period itself* reducing two of the outputs to

$$\begin{aligned} x([n+\frac{1}{2}]) &= h_1[w_4(s_n,s_{n+1})] + h_2[w_5(s_n,s_{n+1})] && (5.16)\\ x([n+1]) &= h_1[w_6(s_n,s_{n+1})] + h_2[w_7(s_n,s_{n+1})]. && (5.17) \end{aligned}$$

This self-dependence is demonstrated notationally with the weighting functions dependent only on the two symbols transmitted during an Alamouti period. Rewritten in vector form (5.16) and (5.17) become

$$\tilde{\mathbf{x}}(s_n,s_{n+1}) = h_1\mathbf{w}^{(1)}(s_n,s_{n+1}) + h_2\mathbf{w}^{(2)}(s_n,s_{n+1}) \qquad (5.18)$$

where we will call $\mathbf{w}^{(1)}$ and $\mathbf{w}^{(2)}$ weighting vectors which can take on 16 different values correspond to each possible combination of s_n and s_{n+1} in a QPSK system. With perfect CSI and in a noiseless system $\tilde{\mathbf{y}}$ is a known quantity for all s_n and s_{n+1}.

Discarding the two corrupted filter outputs for each Alamouti period, the received noisy samples can be written as

$$\mathbf{x}' = \begin{bmatrix} x(n+\frac{1}{2}) \\ x(n+1) \end{bmatrix}. \qquad (5.19)$$

Since $\tilde{\mathbf{x}}$ is a deterministic quantity and now matches the dimensionality of $\mathbf{x}'$, minimizing the error can be achieved with

$$\hat{\mathbf{x}} = \min_{s_n, s_{n+1}} ||\mathbf{x}' - \tilde{\mathbf{x}}(s_n, s_{n+1})||, \tag{5.20}$$

where the values of s_n and s_{n+1} that correspond to the minimizing value are deemed the detected symbols.

The basis vectors $\mathbf{w}^{(1)}$ and $\mathbf{w}^{(2)}$ can be found by either using (5.10) and an estimate for $R_p(\tau)$ or by numerical analysis. For the second case the channel coefficients are set to $h_1 = 1$ and $h_2 = 0$ and a simulation of the system is used to compute $\tilde{\mathbf{x}}$ for every possible symbol combination with noise neglected. The vector $\mathbf{w}^{(1)}$ was found by sampling the uncorrupted filter outputs from (5.16) and (5.17). A similar method is used to find $\mathbf{w}^{(2)}$.

5.4.2 Trellis Detection

A second detection method can be constructed by first defining the quantity $\boldsymbol{\Delta}$ as

$$\boldsymbol{\Delta} = \hat{\mathbf{x}} - \mathbf{x} \tag{5.21}$$

where $\mathbf{x}$ are all four of the received outputs and $\hat{\mathbf{x}}$ are the estimates as calculated from (5.10). A solution can be found by minimizing $|\boldsymbol{\Delta}|^2$ for each Alamouti period. In [5] it was suggested that using the Viterbi algorithm (VA) is a possible method to minimize $|\boldsymbol{\Delta}|^2$ and thereby detect symbols transmitted with Alamouti's scheme in a(n) (S)OQPSK system. The VA is performed for this scenario by assigning each possible matched filter output $\{x(n+\frac{1}{2}), x(n+1), x(n+\frac{3}{2})\, x(n+2)\}$ as a state in the trellis. The observed MF outputs are then used as path metrics versus each state. After the last 16 path metrics are evaluated the path with the lowest cost is deemed the detected bits $(\hat{a}_n, \hat{b}_n, \hat{a}_{n+1}, \hat{b}_{n+1})$. The VA is then repeated for the next four MF outputs. A possible trellis that merges Alamouti transmission and the VA is shown in Figure 5.3.

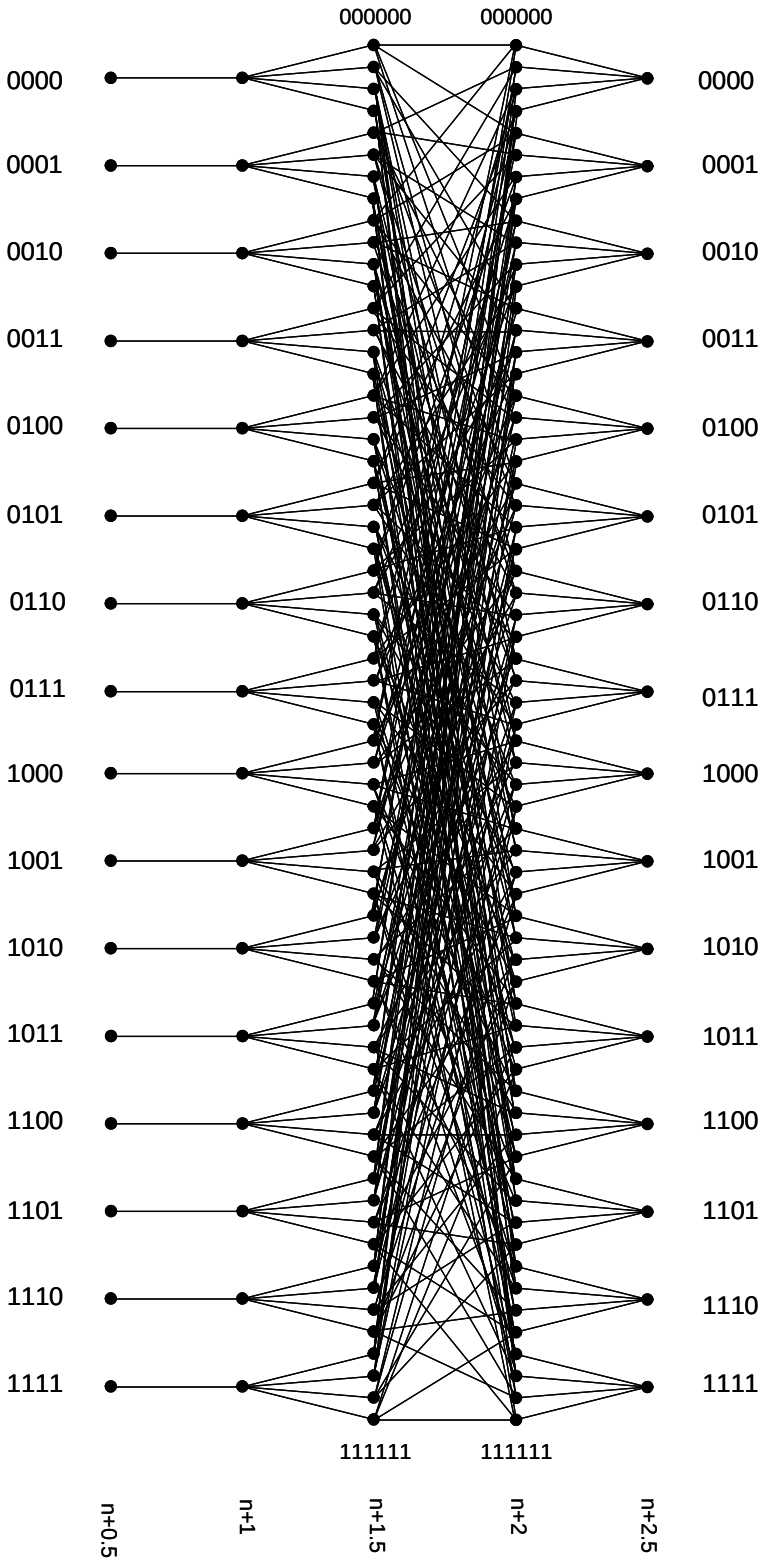

Figure 5.3: Trellis for Viterbi Algorithm.

The elements of $\mathbf{\Delta}$ can be rewritten for each output block as

$$\Delta = \begin{bmatrix} \Delta(n+\frac{1}{2}) \\ \Delta(n+1) \\ \Delta(n+\frac{3}{2}) \\ \Delta(n+2) \end{bmatrix} = \begin{bmatrix} \hat{x}(n+\frac{1}{2}) - x(n+\frac{1}{2}) \\ \hat{x}(n+1) - x(n+1) \\ \hat{x}(n+\frac{3}{2}) - x(n+\frac{3}{2}) \\ \hat{x}(n+2) - x(n+2) \end{bmatrix} \tag{5.22}$$

with the branch metric for the trellis becoming

$$\lambda_{n+\frac{1}{2}}(a_n, b_n, a_{n+1}, b_{n+1}) = |\Delta(n+\frac{1}{2})|^2 \tag{5.23}$$

$$\lambda_{n+1}(a_n, b_n, a_{n+1}, b_{n+1}) = |\Delta(n+1)|^2 \tag{5.24}$$

$$\lambda_{n+\frac{3}{2}}(a_n, b_n, a_{n+1}, b_{n+1}, a_{n+2}, a_{n+3}) = |\Delta(n+\frac{3}{2})|^2 \tag{5.25}$$

$$\lambda_{n+2}(b_n, b_{n+1}, a_{n+2}, b_{n+2}, a_{n+3}, b_{n+3}) = |\Delta(n+2)|^2. \tag{5.26}$$

After defining the trellis path and branch metrics the VA can be used to find the minimum path to the final state. The VA will work down the trellis eliminating duplicate paths and finishing with a minimum path cost for each of the 16 final states. The starting point to the path with the minimum cost is the chosen solution. The next block of four outputs will then have initial path costs from the ending path costs of the previous states.

Figure 5.4 contains plots of SISO SOQPSK transmission along with the simple detector and detection using the VA. Notice how the VA performs nearly as well as the SISO case while the performance of the simple detector is reduced due to the fact that half the received information is neglected in the computation.

5.5 SOQPSK DSTM Detection

DSTM is similar to Alamouti's code in that it requires a special symbol mapping over space and time. Differentially encoded blocks can be written as

$$\mathbf{C}_k = \begin{bmatrix} s_n^{(1)} & s_{n+1}^{(1)} \\ s_n^{(2)} & s_{n+1}^{(2)} \end{bmatrix} \tag{5.27}$$

where s are QPSK symbols, the subscript k denotes transmit time, and the superscript corresponds to the appropriate transmit channel. Evaluation of this code reveals that,

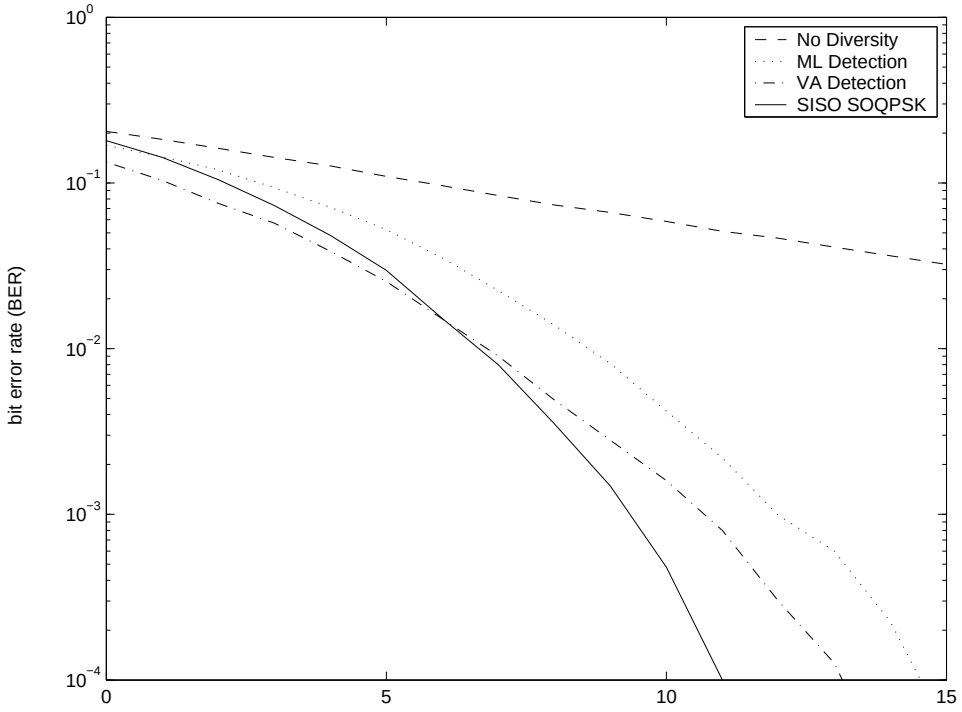

Figure 5.4: Alamouti detection for SOQPSK transmission.

like Alamouti, DSTM requires modification if it is to function in connection with the ARTM SOQPSK transmitter. In a similar manner as Eq. (5.9), update equations can be created to pre-encode data bits such that the necessary symbols are transmitted after differential bit encoding, ternary symbol mapping, and frequency modulation. Confidence in being able to transmit the symbols populating matrix blocks allows us to examine the receiver for possible detection schemes.

One difficulty associated with detecting DSTM blocks transmitted from an OQPSK system is easily seen by examining the detector required for DSTM, Eq. (4.7), written in the mathematically equivalent form

$$\begin{aligned} \hat{\mathbf{G}_k} &= \arg\max_{\mathbf{G}\in\mathcal{G}} \mathrm{ReTr}\left\{\mathbf{G}\mathbf{Y}_k^{\dagger}\mathbf{Y}_{k-1}\right\} \\ &= \arg\min_{\mathbf{G}\in\mathcal{G}} ||\mathbf{Y}_{k-1} - \mathbf{Y}_k\mathbf{G}^{\dagger}||^2. \end{aligned} \tag{5.28}$$

A simplistic view of DSTM detection gives insight into problems associated with OQPSK. Due to the group nature of $\mathcal{G}$, in a noiseless system $\mathbf{Y}_{k-1} = \mathbf{H}\mathbf{C}_{k-1}$ and $\mathbf{Y}_k = \mathbf{H}\mathbf{C}_{k-1}\mathbf{G}_k$ which leads to a minimum error when $\mathbf{Y}_{k-1} = \mathbf{Y}_k\mathbf{G}_k^{\dagger}$ (yielding the detected block $\mathbf{G}_k$). This is valid in a non-offset modulation scheme but is *not* valid with OQPSK for two reasons. First, the dimensionality of $\mathbf{Y}_k$ (1x4) for OQPSK is twice that of non-offset QPSK (1x2) since signals are sampled twice per symbol period, which invalidates the matrix multiplies necessary in DSTM detection. Second, symbol values are "smeared" across filter outputs at the receiver as was shown in Eq. (5.10) resulting in $\mathbf{Y}_{k-1} \neq \mathbf{Y}_k\mathbf{G}_k^{\dagger}$ even if the dimensionality of $\mathbf{Y}_k$ could be fixed.

Explicit expressions for the receiver output samples for DSTM modulation are similar to those produced by Alamouti's scheme in an offset system. Consider the standard differentially encoded block $\mathbf{C}_k$ obtained from the symbol transmission sequence shown in Table 4.1. This transmitted block will produce the following output

estimates given an offset modulation scheme

$$\mathbf{Y}_k = \begin{bmatrix} h_1[a_n^{(1)} + jR_p(\frac{T_s}{2})b_{n-1}^{(1)} + R_p(\frac{-T_s}{2})b_n^{(1)}] + h_2[a_{n+1}^{(2)} + R_p(\frac{T_s}{2})b_{n-2}^{(2)} + R_p(\frac{-T_s}{2})b_{n+1}^{(2)}] \\ h_1[jb_n + R_p(\frac{T_s}{2})a_n - R_p(\frac{-T_s}{2})a_{n+1}^{(1)}] + h_2[jb_{n+1}^{(2)} + R_p(\frac{T_s}{2})a_{n+1}^{(2)} - R_p(\frac{-T_s}{2})a_n^{(2)}] \\ h_1[a_{n+1}^{(1)} + jR_p(\frac{T_s}{2})b_n^{(1)} + R_p(\frac{-T_s}{2})b_{n+1}^{(1)}] + h_2[a_{n+2}^{(2)} + R_p(\frac{T_s}{2})b_{n-1}^{(2)} + R_p(\frac{-T_s}{2})b_{n+2}^{(2)}] \\ h_1[jb_{n+1} + R_p(\frac{T_s}{2})a_{n+1} - R_p(\frac{-T_s}{2})a_{n+2}^{(1)}] + h_2[jb_{n+2}^{(2)} + R_p(\frac{T_s}{2})a_{n+2}^{(2)} - R_p(\frac{-T_s}{2})a_{n+1}^{(2)}] \end{bmatrix}. \tag{5.29}$$

Eq. (5.29) verifies the aforementioned detection problems for (S)OQPSK DSTM transmission by demonstrating the change in dimensionality as well as the loss of orthogonality of the received block.

A non-optimal yet simple solution to both of these problems is to add adjacent outputs over a symbol time (i.e. adding consecutive rows from Eq. (5.29)). This reduces the four outputs per matrix to two with the following values:

$$\mathbf{Y}_k = \begin{bmatrix} h_1[a_n^{(1)} + jR_p(\frac{T_s}{2})b_{n-1}^{(1)} + R_p(\frac{-T_s}{2})b_n^{(1)}] + h_2[a_{n+1}^{(2)} + R_p(\frac{T_s}{2})b_{n-2}^{(2)} + R_p(\frac{-T_s}{2})b_{n+1}^{(2)}] \\ h_1[a_{n+1}^{(1)} + jR_p(\frac{T_s}{2})b_n^{(1)} + R_p(\frac{-T_s}{2})b_{n+1}^{(1)}] + h_2[a_{n+2}^{(2)} + R_p(\frac{T_s}{2})b_{n-1}^{(2)} + R_p(\frac{-T_s}{2})b_{n+2}^{(2)}] \end{bmatrix}. \tag{5.30}$$

The received blocks can be written in matrix form as

$$\mathbf{Y}_k = \alpha \mathbf{H}\mathbf{C}_k + \mathbf{H}\mathbf{S} + \boldsymbol{\eta} \tag{5.31}$$

where $\alpha = 1 + R_p(\frac{T_s}{2})$ (assuming that $R_p(\frac{T_s}{2}) = R_p(\frac{-T_s}{2})$ and $\mathbf{S}$ will hold the remaining terms that occur from symbol overlap in offset modulation. In a noiseless system the affect of the residual matrix $\mathbf{S}$ can be observed from the received constellation element values. Figure 5.5 shows received signals when adjacent filter outputs are summed. Notice how offset modulation schemes push symbols from their ideal constellation locations much as noise would do. This motivates the combination of the residual matrix with the AWGN term

$$\mathbf{Y}_k = \alpha \mathbf{H}\mathbf{C}_k + \boldsymbol{\eta}' \tag{5.32}$$

producing a received matrix that has the same form as though it were transmitted with QPSK modulation. Obviously, detection with Eq. (5.32) will have a lower SNR due to increased noise caused by symbol overlap but use of the standard DSTM

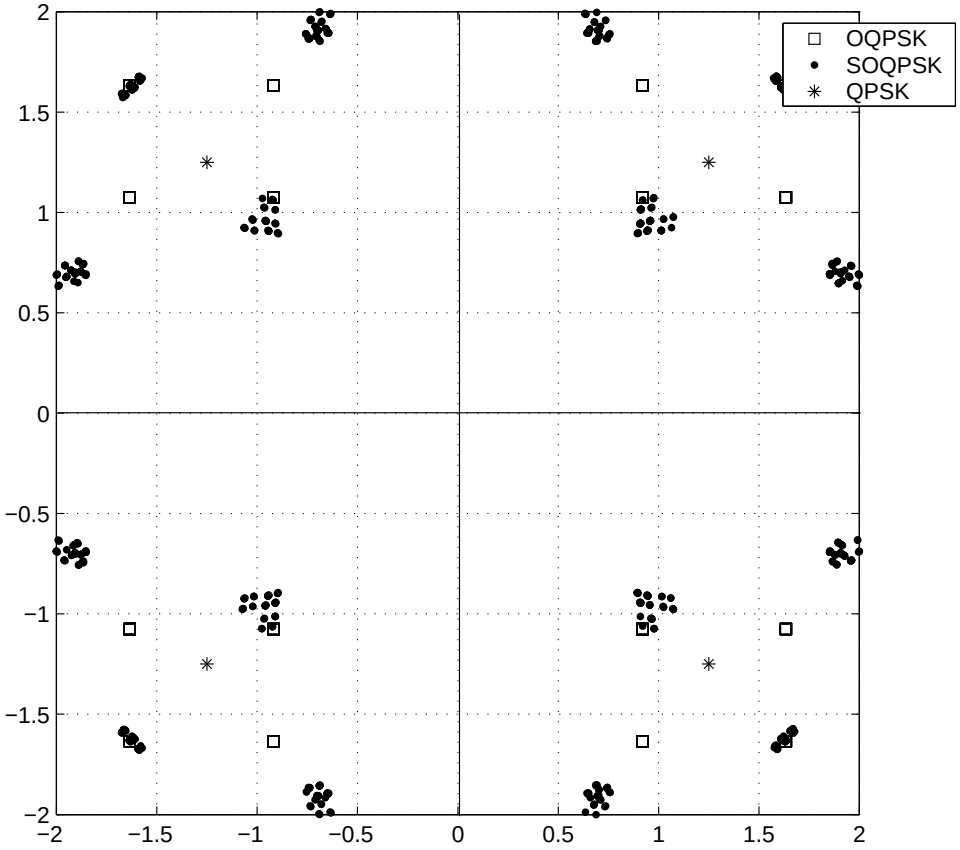

Figure 5.5: Receive symbol constellation for offset modulation given summed adjacent symbols.

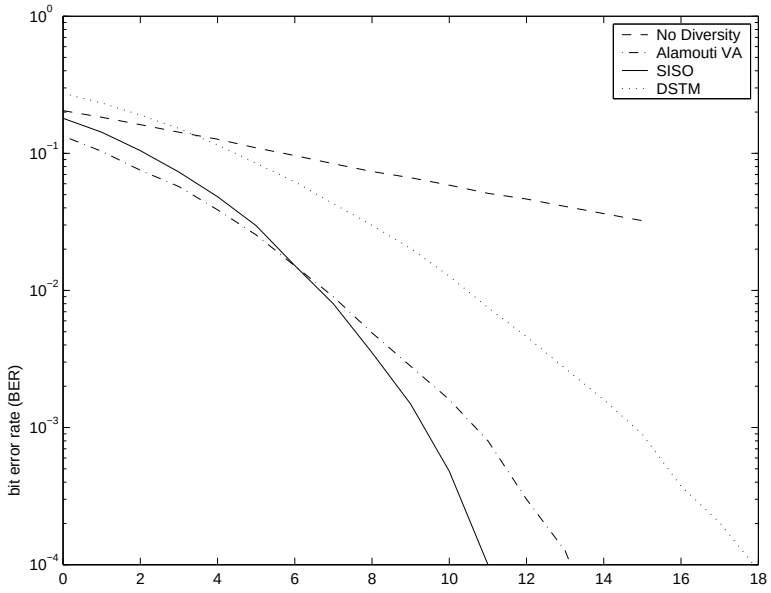

Figure 5.6: Space-time code performance using SOQPSK transmitters.

decoding equation is now possible. Further degradation occurs since the noise is now correlated with the signal suggesting that Eq. (4.7) is not the ML solution for this case. Figure 5.6 shows the performance of space-time codes used with SOQPSK modulation with the detection strategies presented in this chapter.

Chapter 6

Conclusion and Future Work

Accurate flight data from airborne test aircraft assists in technological advancements at government telemetry ranges. Dual-antenna transmission is employed to overcome signal occlusion resultant from highly mobile maneuvers. However, as shown in this work, dual antennas create self-interference which significantly degrades the communication performance. Overcoming this self-interference is necessary for maintaining a reliable wireless telemetry link.

This thesis has demonstrated how the use of space-time codes, originally developed to improve communication in multipath channels, can provide a highly reliable link for the aeronautical telemetry channel. Specifically, Alamouti's code overcomes the interference by producing orthogonal signal transmissions over two symbol periods. This orthogonality of signal transmission compensates for frequent nulls common on antenna arrays and, in fact, produces the same bit error performance as non-occlusive SISO transmission. The drawback of Alamouti's scheme is the need for some degree of channel state information (CSI) accuracy. For a high variability channel Alamouti's scheme requires frequent training intervals, thus reducing the throughput and perhaps precluding its use as a viable transmission scheme.

Differential space-time modulation (DSTM) is similar to Alamouti's code in that it produces orthogonal transmission sequences. However, the advantage of DSTM lies in not requiring any CSI at the receiver thus removing the burden of accurate channel knowledge. Differential detection comes at the cost of transmitting at a fraction of the rate of Alamouti's scheme.

Adding transmit diversity to a dual-antenna system is beneficial to overall bit error rate performance as well as link integrity. These benefits are not constrained to linear modulation schemes such as QPSK but have been shown to work for offset type modulations as well. Though shown to be successful, there is still much research available to further the use of space-time codes in overcoming antenna self-interference.

1. Optimal (S)OQPSK DSTM detection. A sub-optimal DSTM detector for (S)OQPSK waveforms was presented in this thesis. Though producing adequate results, the performance of this detector is significantly worse than that of a SISO QPSK system.

2. Rate 2 DSTM coding scheme. The major drawback of DSTM with QPSK symbols is that is operates at rate 1.5 compared to Alamouti's scheme rate 2 operation. It would be useful to create a rate 2 DSTM scheme based on QPSK symbols, although it is not clear that this is possible.

3. Configurable transmitter/receiver hardware. Ideally, a circuit could be designed that is able to switch between using Alamouti's code and DSTM for testing purposes. This circuit would need to be easily configurable and work with pre-existing hardware.

4. Analytic BER curves for DSTM. Analytic BER solutions for Alamouti's code derived in this thesis enable simple performance assessment. Similar BER solutions for DSTM would be ideal and would provide similar benefits.

5. Dual-antenna differential delay. All simulations in this thesis assumed signals were transmitted simultaneously from both antennas. Realistically, there is a small differential delay, denoted τ, introduced into the channel due to unequal cable lengths between transmitters and antennas as well as the unequal path lengths from the transmit antennas to the receiver. This differential delay will affect the channel as

$$\begin{aligned} h_1(t') &= h_1(t) \\ h_2(t') &= h_2(t-\tau), \end{aligned} \tag{6.1}$$

where sampled outputs will be based on the time variable t'. With τ sufficiently large further distortion will occur at the receiver.

Appendix

Appendix A

Channel Model

In this thesis two types of channel models are used. The first is a Rayleigh channel where the channel coefficients are drawn from a complex Gaussian random variable. The second is a telemetry channel model which calculates the actual magnitude and phase coefficients of the channel given specific aircraft attitudes and using electromagnetic theory. The telemetry channel model is used most often and will be the case unless specifically stated otherwise.

A.1 Telemetry Channel

One goal of this thesis is to obtain an accurate model representation of a real life aircraft situation. Such a model is of supreme importance as it gives confidence in the accuracy of mathematical simulations. We start by placing the transmit antennas at (x_1, y_1, z_1) and (x_2, y_2, z_2) respectively, where (x_i, y_i, z_i) for $i \in 1, 2$ are measured from the local coordinate frame whose origin is at the center of the aircraft. The receive ground station antenna is located at the spherical coordinates (r, θ, ϕ) which are also measured from the center of the aircraft but lie in the global coordinate frame. In standard flight tests the aircraft attitude will be continually changing whereas the receive antenna will be considered fixed. In order to obtain correct values we need to place the receive coordinates in the same frame as the transmit coordinates. This can be accomplished by using the Cardanian transformation matrix

$$T = \begin{bmatrix} c(\beta)c(\gamma) & s(\alpha)s(\beta)c(\gamma) + c(\alpha)s(\gamma) & -c(\alpha)s(\beta)c(\gamma) + s(\alpha)s(\gamma) \\ -c(\beta)s(\gamma) & -s(\alpha)s(\beta)s(\gamma) + c(\alpha)c(\gamma) & c(\alpha)s(\beta)s(\gamma) + s(\alpha)s(\gamma) \\ s(\beta) & -s(\alpha)c(\beta) & c(\alpha)c(\beta) \end{bmatrix} \quad \text{(A.1)}$$

where $c\{\cdot\}$ denotes the cosine operator and $s\{\cdot\}$ denotes the sine operator. This matrix is defined by the three rotation angles (α, β, γ) which are the rotations used around the x, y, and z axes respectively to place the global coordinate frame in line with the local coordinate frame. For example, if the receiver was at a point (x_g, y_g, z_g) in the global frame and the aircraft was at a certain attitude defined by $(\alpha_l, \beta_l, \gamma_l)$ the global point can be mapped onto the local frame using (A.1) and

$$\begin{bmatrix} x_l \\ y_l \\ z_l \end{bmatrix} = T \begin{bmatrix} x_g \\ y_g \\ z_g \end{bmatrix} \tag{A.2}$$

where the global point is now at the local point (x_l, y_l, z_l). After performing the Cardanian transformation a simple Cartesian to spherical mapping can be done to produce the desired (r, θ, ϕ) coordinates.

With all geometrical values in the same coordinate frame it is possible to create a transfer function from each transmit antenna to the receive antenna

$$h_i \quad = \quad A(\theta, \phi) e^{jk(x_i \sin\theta \cos\phi + y_i \sin\theta \sin\phi + z \cos\theta)} \tag{A.3}$$

with $k = 2\pi/\lambda$ as the free-space wavenumber and λ the wavelength. $A(\theta, \phi)$ is the amplitude pattern and represents magnitude loss due to the radiation pattern and aircraft masking. These patterns are shown in Figure A.1. The standard e^{-jkr}/r term has been neglected as it is the same for both antennas and any power loss due to distance from the receive is accounted for in the signal-to-noise ratio.

A.2 Air Vehicle Flight Path

With the channel coefficients defined in (A.3) it is a simple matter to produce realistic flight paths for simulation. Unless otherwise stated all simulations in this thesis use the following conditions

$$\begin{aligned} x_0 &= 0 \\ y_0 &= 0 \\ z_0 &= 1000 \end{aligned} \tag{A.4}$$

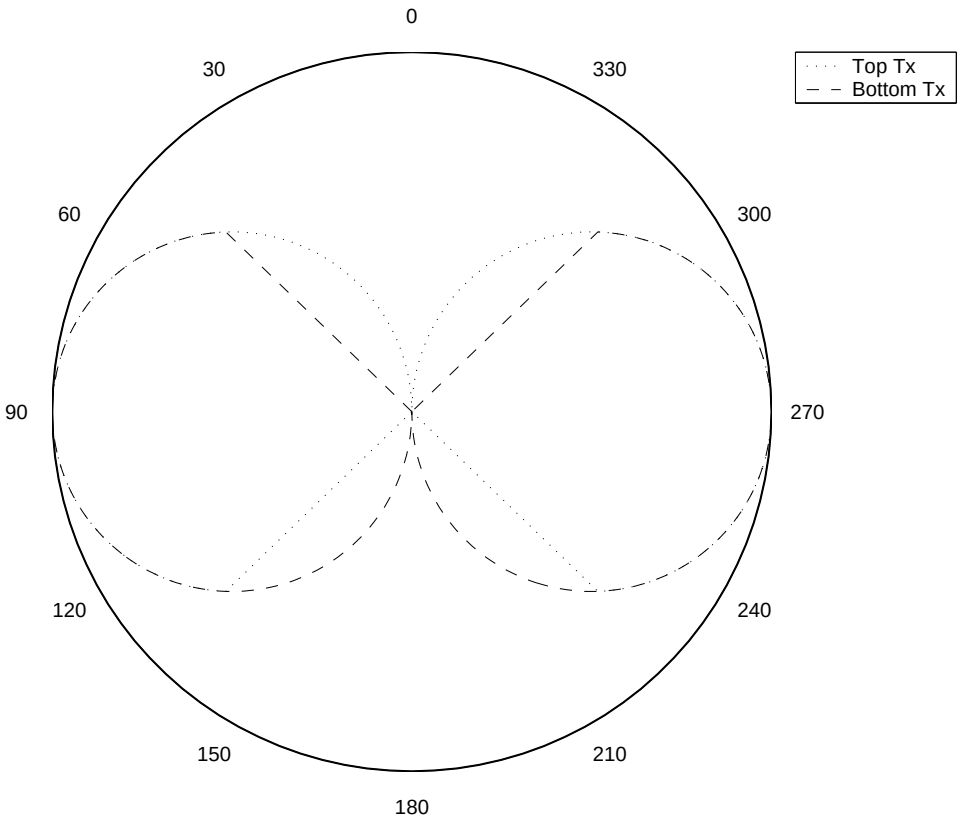

Figure A.1: Radiation patterns from transmit antennas above and below aircraft.

with all values measured in meters. The aircraft moves uniformally in the xyz plane at 200mps

$$d_i(t) = i_0 + 200t \quad , \quad i = x, y, z. \tag{A.5}$$

for an aggregate velocity of 346mps (760 mph). The aircraft also performs a roll of one revolution per second around its center given by

$$\gamma(t) = 2\pi t \tag{A.6}$$

where γ is measured in radians and represents the aforementioned angle for the Cardanian transformation. Using equations (A.4) and (A.5) in (A.3) produces a channel update equation as a function of time

$$h(t) \quad = \quad e^{jk[x\sin\theta(t)\cos\phi(t)+y\sin\theta(t)\sin\phi(t)+z\cos\theta(t)]}. \tag{A.7}$$

The angular update equations can be found by defining a vector $\rho(t)$ for the distance from aircraft center to receive antenna center

$$\rho(t) \quad = \quad \begin{bmatrix} x(t) \\ y(t) \\ z(t) \end{bmatrix} = \begin{bmatrix} x_0 + v_x t \\ y_0 + v_y t \\ z_0 + v_z t \end{bmatrix}. \tag{A.8}$$

The vector $\rho(t)$ can then be brought into the aircrafts local coordinate frame by the Cardanian transformation

$$\rho'(t) = \begin{bmatrix} x'(t) \\ y'(t) \\ z'(t) \end{bmatrix} = T\rho(t). \tag{A.9}$$

After the standard Cartesian to spherical transformation

$$\begin{aligned} r'(t) &= \sqrt{x'(t)^2 + y'(t)^2 + z'(t)^2} \\ \theta'(t) &= \cos^{-1}(z'(t)/r'(t)) \\ \phi'(t) &= \tan^{-1}(y'(t)/x'(t)) \end{aligned} \tag{A.10}$$

all equations have been derived to produce channel coefficients for each channel as a function of time.

A.3 Rayleigh Channel

For Rayleigh channels, the received signal is formulated exactly as the telemetry channel received signal

$$\mathbf{r} = \mathbf{H}\mathbf{x} + \boldsymbol{\eta} \tag{A.11}$$

where H is instead populated by samples drawn from a zero mean complex Gaussian random variable.

Bibliography

[1] S. M. Alamouti, "A simple transmit diversity technique for wireless communications," *IEEE J. Selected Areas Commun.*, vol. 16, pp. 1451–1458, Oct. 1998.

[2] B. L. Hughes, "Differential space-time modulation," *IEEE Trans. Inf. Theory*, vol. 46, pp. 2567–2578, Nov. 2000.

[3] J. G. Proakis, *Digital Communications*, McGraw-Hill, 1995.

[4] A. Shokrollahi, B. Hassibi, B. M. Hochwald, and W. Sweldens, "Representation theory for high-rate multiple-antenna code design," *IEEE Trans. Inf. Theory*, vol. 47, pp. 2335–2367, Sept. 2001.

[5] T. Nelson, "Space-time coded soqpsk in the presence of differential delays," in *Proc. of the 2004 Intl. Telemetry Conference*, San Diego, CA, Oct. 18-21 2004.